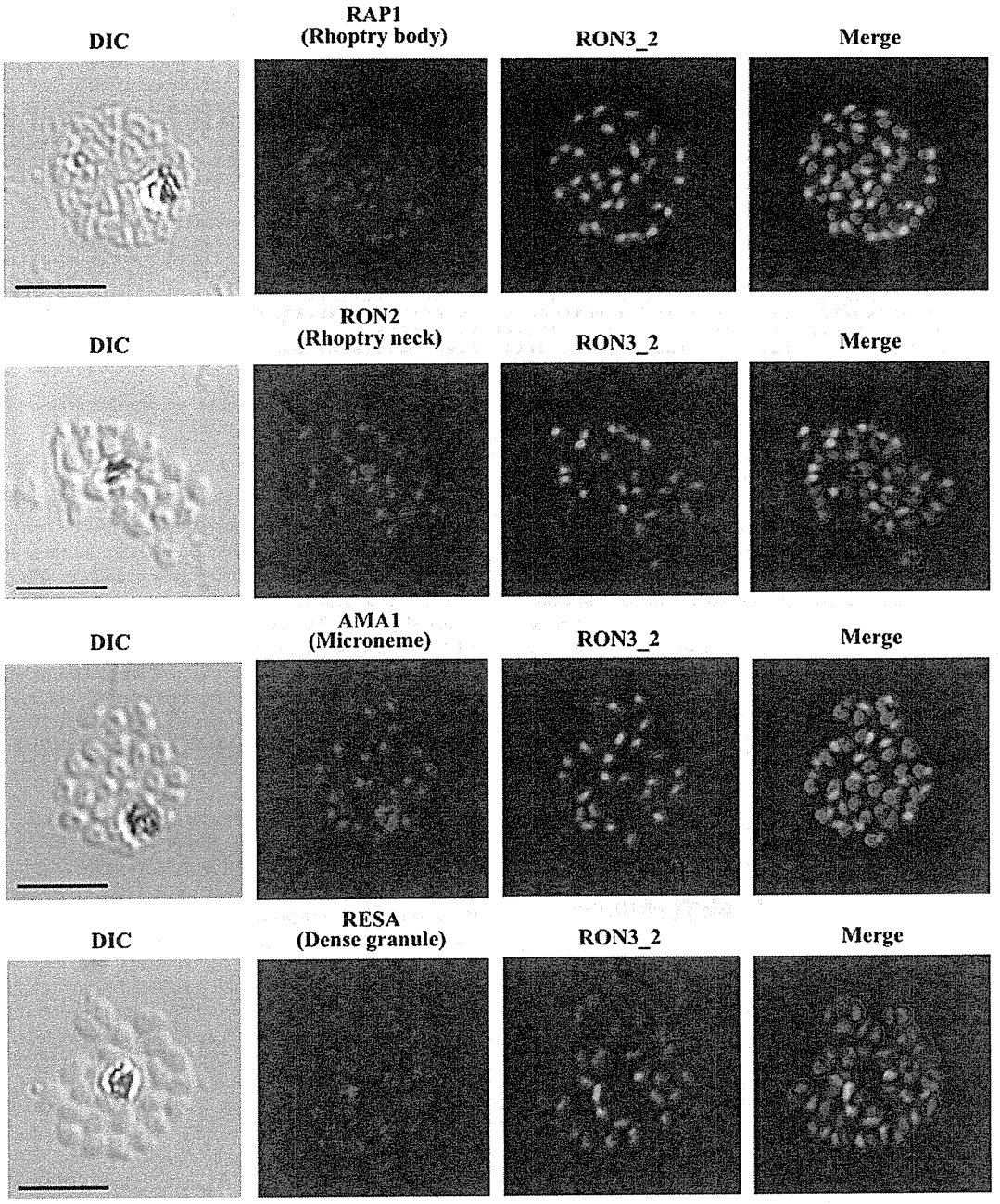

Fig. 4. *Pf*RON3 is expressed at the apical end of *Plasmodium* merozoites. Schizont and merozoite stage parasites were dual-labeled with antisera against *Pf*RON3_2 and either *Pf*RAP1 (rhoptry body marker), *Pf*RON2 (rhoptry neck marker), *Pf*AMA1 (microneme marker), or *Pf*RESA (dense granule marker). Nuclei are visualized with DAPI in merged images shown in the right panels. Bars represent 5 μm.

localization of *Pf*RON3 and the timing of the novel complex formation during the merozoite invasion process. Hence, the role of *Pf*RON3 and the novel complex in formation of the moving junction and the merozoite invasion process could not be elucidated. It will be interesting to undertake further experiments to shed light on the localization and function of *Pf*RON3 and the novel complex during merozoite invasion.

In summary, our results show that *Pf*RON3 is a rhoptry body protein, not a rhoptry neck protein, and that it interacts with *Pf*RON2 and *Pf*RON4, but not with *Pf*AMA1. These results suggest that *Pf*RON3 partakes in the novel *Pf*RON complex formation (*Pf*RON2, 3, and 4), but not in formation of the moving junction complex (*Pf*RON2, 4, 5, and *Pf*AMA1). The novel *Pf*RON complex, as well as the moving junction complex, might play a fundamental role in erythrocyte invasion by merozoite stage parasites.

Acknowledgments

We are grateful to Jean F. Dubremetz for providing the anti-*Pf*RON4 monoclonal antibody, Robin F. Anders for providing the anti-*Pf*RESA monoclonal antibody, and Niwat Kangwanrangsan for providing the mouse anti-*Pf*EXP2 antibody. We thank Masachika Shudo and Keizou Oka, Integrated Center for Science, Ehime University, Japan for technical assistance. We thank Thangavelu U. Arumugam for critical

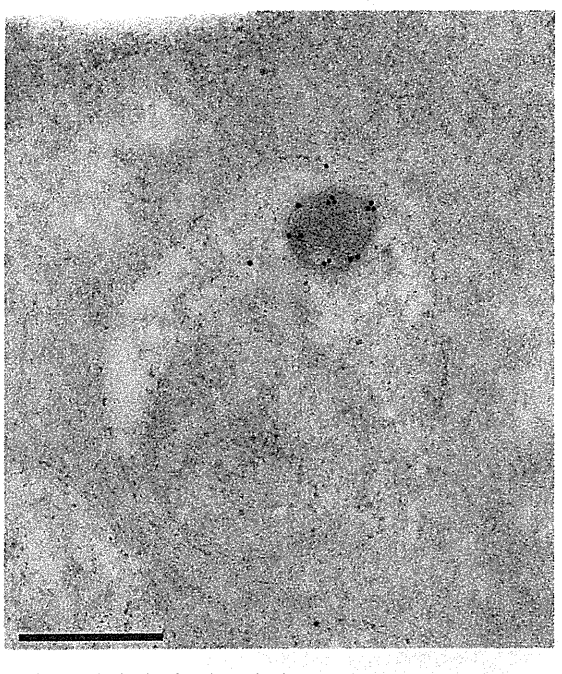

Fig. 5. Rhoptry body localization of *Pf*RON3 by immunoelectron microscopy. Longitudinally sectioned merozoites in mature schizonts were labeled with rabbit anti-*Pf*RON3_2 antibodies followed by secondary antibody conjugated with gold particles. The image shows that the gold particle signals were restricted to the merozoite rhoptry body. Bar represents 500 nm.

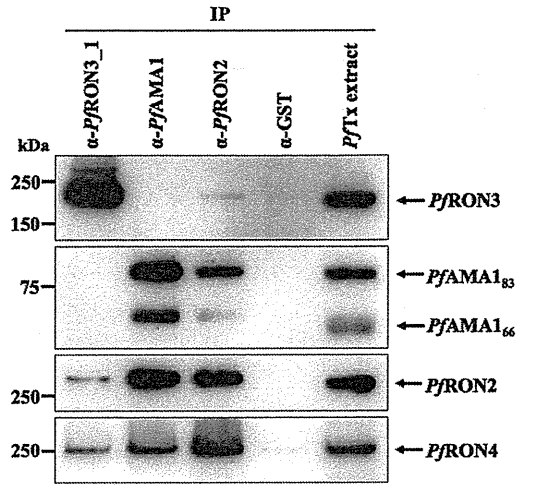

Fig. 7. *Pf*RON3 is not involved in the RON–AMA1 complex. Triton X-100 extracts of schizont-rich parasite (*Pf*Tx extract) were immunoprecipitated (IP) with rabbit sera against *Pf*RON3 (α-*Pf*RON3_1), *Pf*AMA1 (α-*Pf*AMA1), *Pf*RON2 (α-*Pf*RON2), or GST (α-GST), then stained with mouse antisera against *Pf*RON3, *Pf*AMA1, *Pf*RON2, or *Pf*RON4, respectively. Immunoprecipitation using anti-GST antibody was used as a negative control. No bands were detected in the anti-GST immunoprecipitate, indicating the exclusion of potential carryover of proteins due to insufficient or inadequate washing steps.

reading of the manuscript. This research was supported by the Ministry of Education, Culture, Sports, Science and Technology (21249028 and 21022034), and by the Ministry of Health, Labour,

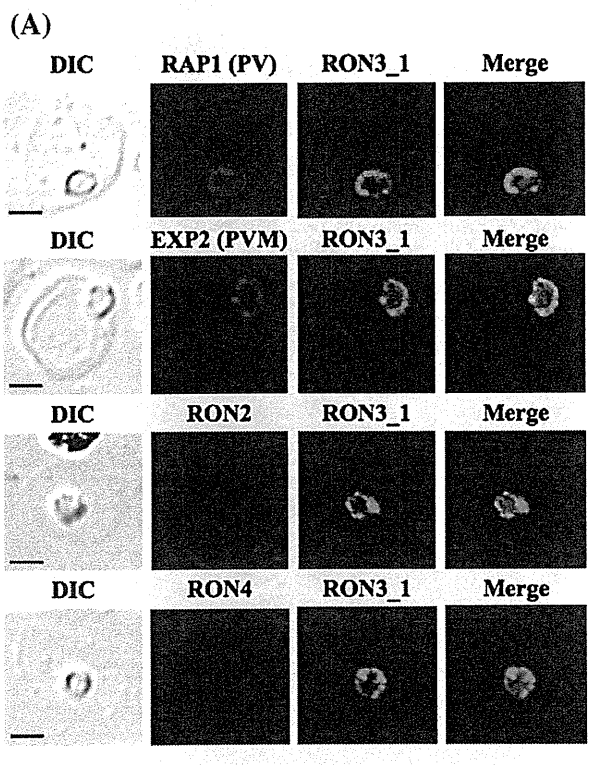

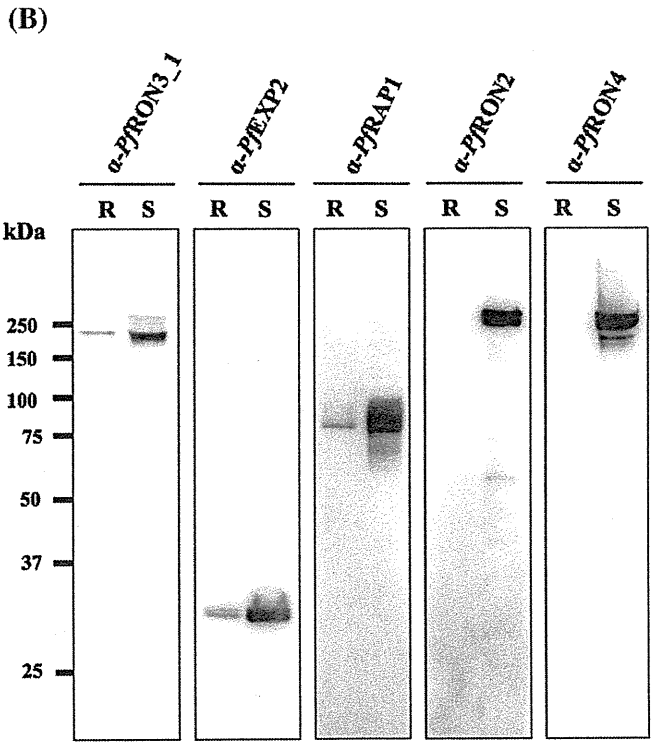

Fig. 6. *Pf*RON3 is found in the parasitophorous vacuole in ring stage parasites. (A) Ring stage parasites were dual-labeled with antisera against *Pf*RON3_1 and either *Pf*RAP1 (PV marker), *Pf*EXP2 (PVM marker), *Pf*RON2, or *Pf*RON4. Nuclei are visualized with DAPI in merged images shown in the right panels. Bars represent 2.5 μm. (B) Proteins from synchronized parasite cultures were harvested at the ring stage (R) and schizont stage (S), and separated by SDS-PAGE on a 12.5% gel under a reducing condition. After transfer of proteins onto a PVDF membrane, the membrane was stained using rabbit anti-*Pf*RON3_1, mouse anti-*Pf*RAP1, anti-*Pf*EXP2, anti-*Pf*RON2, anti-*Pf*RON4 antibodies.

and Welfare, Japan (H20-Shinkou-ippan-013 and H21-Chikyukibo-ippan-005).

Appendix A. Supplementary data

Supplementary data to this article can be found online at doi:10.1016/j.parint.2011.01.001.

References

[1] Hay SI, Guerra CA, Gething PW, Patil AP, Tatem AJ, Noor AM, et al. A world malaria map: *Plasmodium falciparum* endemicity in 2007. PLoS Med 2009;6:e1000048.
[2] Cowman AF, Crabb BS. Invasion of red blood cells by malaria parasites. Cell 2006;124:755–66.
[3] Kaneko O. Erythrocyte invasion: vocabulary and grammar of the *Plasmodium* rhoptry. Parasitol Int 2007;56:255–62.
[4] Aikawa M, Miller LH, Johnson J, Rabbege J. Erythrocyte entry by malarial parasites. A moving junction between erythrocyte and parasite. J Cell Biol 1978;77:72–82.
[5] Lebrun M, Michelin A, El Hajj H, Poncet J, Bradley PJ, Vial H, et al. The rhoptry neck protein RON4 re-localizes at the moving junction during *Toxoplasma gondii* invasion. Cell Microbiol 2005;7:1823–33.
[6] Alexander DL, Mital J, Ward GE, Bradley P, Boothroyd JC. Identification of the moving junction complex of *Toxoplasma gondii*: a collaboration between distinct secretory organelles. PLoS Pathog 2005;1:e17.
[7] Alexander DL, Arastu-Kapur S, Dubremetz JF, Boothroyd JC. *Plasmodium falciparum* AMA1 binds a rhoptry neck protein homologous to *Tg*RON4, a component of the moving junction in *Toxoplasma gondii*. Eukaryot Cell 2006;5:1169–73.
[8] Cao J, Kaneko O, Thongkukiatkul A, Tachibana M, Otsuki H, Gao Q, et al. Rhoptry neck protein RON2 forms a complex with microneme protein AMA1 in *Plasmodium falciparum* merozoites. Parasitol Int 2009;58:29–35.
[9] Richard D, MacRaild CA, Riglar DT, Chan JA, Foley M, Baum J, et al. Interaction between *Plasmodium falciparum* apical membrane antigen 1 and the rhoptry neck protein complex defines a key step in the erythrocyte invasion process of malaria parasites. J Biol Chem 2010;285:14815–22.
[10] Triglia T, Healer J, Caruana SR, Hodder AN, Anders RF, Crabb BS, et al. Apical membrane antigen 1 plays a central role in erythrocyte invasion by *Plasmodium* species. Mol Microbiol 2000;38:706–18.
[11] Hehl AB, Lekutis C, Grigg ME, Bradley PJ, Dubremetz JF, Ortega-Barria E, et al. *Toxoplasma gondii* homologue of *Plasmodium* apical membrane antigen 1 is involved in invasion of host cells. Infect Immun 2000;68:7078–86.
[12] Bradley PJ, Ward C, Cheng SJ, Alexander DL, Coller S, Coombs GH, et al. Proteomic analysis of rhoptry organelles reveals many novel constituents for host–parasite interactions in *Toxoplasma gondii*. J Biol Chem 2005;280:34245–58.
[13] Trager W, Jensen JB. Human malaria parasites in continuous culture. Science 1976;193:673–5.
[14] Tsuboi T, Takeo S, Iriko H, Jin L, Tsuchimochi M, Matsuda S, et al. Wheat germ cell-free system-based production of malaria proteins for discovery of novel vaccine candidates. Infect Immun 2008;76:1702–8.
[15] Tsuboi T, Takeo S, Sawasaki T, Torii M, Endo Y. An efficient approach to the production of vaccines against the malaria parasite. Meth Mol Biol 2010;607:73–83.
[16] Tsuboi T, Takeo S, Arumugam TU, Otsuki H, Torii M. The wheat germ cell-free protein synthesis system: a key tool for novel malaria vaccine candidate discovery. Acta Trop 2010;114:171–6.
[17] Culvenor JG, Day KP, Anders RF. *Plasmodium falciparum* ring-infected erythrocyte surface antigen is released from merozoite dense granules after erythrocyte invasion. Infect Immun 1991;59:1183–7.
[18] Hiller NL, Akompong T, Morrow JS, Holder AA, Haldar K. Identification of a stomatin orthologue in vacuoles induced in human erythrocytes by malaria parasites. A role for microbial raft proteins in apicomplexan vacuole biogenesis. J Biol Chem 2003;278:48413–21.
[19] Kaneko O, Fidock DA, Schwartz OM, Miller LH. Disruption of the C-terminal region of EBA-175 in the Dd2/Nm clone of *Plasmodium falciparum* does not affect erythrocyte invasion. Mol Biochem Parasitol 2000;110:135–46.
[20] Torii M, Adams JH, Miller LH, Aikawa M. Release of merozoite dense granules during erythrocyte invasion by *Plasmodium knowlesi*. Infect Immun 1989;57:3230–3.
[21] Aikawa M, Atkinson CT. Immunoelectron microscopy of parasites. Adv Parasitol 1990;29:151–214.
[22] Altschul SF, Madden TL, Schaffer AA, Zhang J, Zhang Z, Miller W, et al. Gapped BLAST and PSI-BLAST: a new generation of protein database search programs. Nucleic Acids Res 1997;25:3389–402.
[23] Bahl A, Brunk B, Crabtree J, Fraunholz MJ, Gajria B, Grant GR, et al. PlasmoDB: the *Plasmodium* genome resource. A database integrating experimental and computational data. Nucleic Acids Res 2003;31:212–5.
[24] Bendtsen JD, Nielsen H, von Heijne G, Brunak S. Improved prediction of signal peptides: SignalP 3.0. J Mol Biol 2004;340:783–95.
[25] Krogh A, Larsson B, von Heijne G, Sonnhammer EL. Predicting transmembrane protein topology with a hidden Markov model: application to complete genomes. J Mol Biol 2001;305:567–80.
[26] Schultz J, Milpetz F, Bork P, Ponting CP. SMART, a simple modular architecture research tool: identification of signaling domains. Proc Natl Acad Sci USA 1998;95:5857–64.
[27] Thompson JD, Higgins DG, Gibson TJ. CLUSTAL W: improving the sensitivity of progressive multiple sequence alignment through sequence weighting, position-specific gap penalties and weight matrix choice. Nucleic Acids Res 1994;22:4673–80.
[28] Baldi DL, Andrews KT, Waller RF, Roos DS, Howard RF, Crabb BS, et al. RAP1 controls rhoptry targeting of RAP2 in the malaria parasite *Plasmodium falciparum*. EMBO J 2000;19:2435–43.
[29] Johnson D, Gunther K, Ansorge I, Benting J, Kent A, Bannister L, et al. Characterization of membrane proteins exported from *Plasmodium falciparum* into the host erythrocyte. Parasitology 1994;109(Pt 1):1–9.
[30] Fischer K, Marti T, Rick B, Johnson D, Benting J, Baumeister S, et al. Characterization and cloning of the gene encoding the vacuolar membrane protein EXP-2 from *Plasmodium falciparum*. Mol Biochem Parasitol 1998;92:47–57.
[31] Proellocks NI, Coppel RL, Waller KL. Dissecting the apicomplexan rhoptry neck proteins. Trends Parasitol 2010;26:297–304.
[32] Sam-Yellowe TY, Shio H, Perkins ME. Secretion of *Plasmodium falciparum* rhoptry protein into the plasma membrane of host erythrocytes. J Cell Biol 1988;106:1507–13.
[33] Howard RF, Stanley HA, Campbell GH, Reese RT. Proteins responsible for a punctate fluorescence pattern in *Plasmodium falciparum* merozoites. Am J Trop Med Hyg 1984;33:1055–9.
[34] Topolska AE, Lidgett A, Truman D, Fujioka H, Coppel RL. Characterization of a membrane-associated rhoptry protein of *Plasmodium falciparum*. J Biol Chem 2004;279:4648–56.
[35] Collins CR, Withers-Martinez C, Hackett F, Blackman MJ. An inhibitory antibody blocks interactions between components of the malarial invasion machinery. PLoS Pathog 2009;5:e1000273.
[36] Tsuji M, Mattei D, Nussenzweig RS, Eichinger D, Zavala F. Demonstration of heat-shock protein 70 in the sporozoite stage of malaria parasites. Parasitol Res 1994;80:16–21.

Development of the malaria parasite in the skin of the mammalian host

Pascale Gueirard[a], Joana Tavares[a], Sabine Thiberge[a], Florence Bernex[b], Tomoko Ishino[a,1], Genevieve Milon[c], Blandine Franke-Fayard[d], Chris J. Janse[d], Robert Ménard[a,2], and Rogerio Amino[a]

[a]Unité de Biologie et Génétique du Paludisme, Institut Pasteur, 75724 Paris Cedex 15, France; [b]Institut National de la Recherche Agronomique, UMR955 Génétique Fonctionnelle et Médicale and Unité d'Anatomie Pathologique, Ecole Nationale Vétérinaire d'Alfort, F-94700 Maisons-Alfort, France; [c]Unité d'Immunophysiologie et Parasitisme Intracellulaire, Institut Pasteur, 75724 Paris Cedex 15, France; and [d]Department of Parasitology, Centre of Infectious Diseases, Leiden University Medical Centre, 2300 RC, Leiden, The Netherlands

Edited* by Louis H. Miller, National Institutes of Health, Rockville, MD, and approved September 8, 2010 (received for review July 5, 2010)

The first step of *Plasmodium* development in vertebrates is the transformation of the sporozoite, the parasite stage injected by the mosquito in the skin, into merozoites, the stage that invades erythrocytes and initiates the disease. The current view is that, in mammals, this stage conversion occurs only inside hepatocytes. Here, we document the transformation of sporozoites of rodent-infecting *Plasmodium* into merozoites in the skin of mice. After mosquito bite, ~50% of the parasites remain in the skin, and at 24 h ~10% are developing in the epidermis and the dermis, as well as in the immunoprivileged hair follicles where they can survive for weeks. The parasite developmental pathway in skin cells, although frequently abortive, leads to the generation of merozoites that are infective to erythrocytes and are released via merosomes, as typically observed in the liver. Therefore, during malaria in rodents, the skin is not just the route to the liver but is also the final destination for many inoculated parasites, where they can differentiate into merozoites and possibly persist.

intravital imaging | *Plasmodium* | schizogony

Malarial infection starts with the inoculation of *Plasmodium* sporozoites by mosquitoes probing the vertebrate skin for blood. The highly motile sporozoites eventually invade host target cells where they differentiate and divide into numerous merozoites, the parasite form that invades erythrocytes and initiates the pathogenic phase of malarial infection. The host cell type in which sporozoites transform into merozoites, however, differs between *Plasmodium* species. In species that infect birds, sporozoites differentiate inside macrophages primarily in the skin but also in the spleen, liver, and bone marrow (1). In species that infect mammals, sporozoites are known to differentiate only inside hepatocytes in the liver (2–4).

The first demonstration that sporozoites of mammal-infecting *Plasmodium* species develop inside hepatocytes was made in 1948 after i.v. inoculation of sporozoites of *P. cynomologi* into rhesus monkeys (2). In addition to reporting fully mature parasites inside hepatocytes, the authors also documented the persistence of immature and dormant forms of the parasite in the liver several months after the initial inoculation, which they proposed to be the cause of relapses (5), and were later called hypnozoites (6). Subsequent work indicated that sporozoites of species that infect humans (7) also undergo complete development inside hepatocytes.

Since these early studies, *P. berghei* and the related *P. yoelii* species, which infect rodents, have been used as practical and safe models for studying the pre-erythrocytic phase of malaria. These parasites were shown to differentiate in the liver of laboratory rodents (8), and the *P. berghei*/rodent system was used to demonstrate that the majority of sporozoites were inoculated by mosquitoes in the skin rather than directly into the blood circulation (9), as traditionally assumed. More recently, the generation of fluorescent *P. berghei* parasites, along with the development of intravital imaging approaches applicable to rodents, have allowed rapid progress in our understanding of the fate of *Plasmodium* sporozoites in the mammalian host.

Intravital imaging of *P. berghei* sporozoites confirmed that sporozoites were injected in the skin of the mouse, where they display vigorous motility (10). Quantitative analysis revealed that more than half of the *P. berghei* sporozoites inoculated by mosquitoes in the mouse ear skin were still present at the bite site after 1 h (11), and ~40% stayed as long as 6 h (12), when sporozoites are no longer actively motile. Of the sporozoites that left the mosquito bite site, ~70% were found to take the blood route and ~30% the lymphatic route (11). The latter terminate their journey in the first draining lymph node, where most die in a few hours, though a few develop, at least partially, in association with podoplanin-expressing cells (11). A similar tripartite fate of sporozoites staying in the skin, leaving the skin via the blood or via the lymph, was later also described for *P. yoelii* using quantitative PCR analysis (13).

In this work, we analyze the fate of sporozoites of rodent-infecting *Plasmodium* species in the skin of mice.

Results and Discussion

***P. berghei* Develops Inside Skin Cells in the Mouse.** We first analyzed the fate of the *P. berghei* sporozoites that remain in the skin of the host. *Anopheles stephensi* mosquitoes were allowed to transmit WT green fluorescent sporozoites (14) into the ear of SKH1 *hairless* mice (15), which display little autofluorescence in the skin, and parasites were imaged daily using spinning-disk confocal microscopy (16). Typically, inside hepatocytes, parasites round up and increase their size to become spherical exoerythrocytic forms (EEF) of ~40-μm average diameter, undergo schizogony, and produce thousands of uninucleate merozoites in ~50–70 h (4). Approximately 11% of the elongated sporozoites detected in the skin soon after the bite were still observed after 24 h (day 1, D1) as brightly fluorescent, round parasites (Fig. 1 *A* and *B*). The average size and fluorescence intensity of the EEF steadily increased with time (Fig. 1 *A* and *C*). However, the maximal diameter of skin EEF, typically reached at D3–D4, remained 2–3 times smaller than the maximal diameter of liver EEF, reached at D2 (Fig. 1 *A* and *C*). When parasite survival was assessed after intradermal injection of ~5,000 sporozoites into the ear skin, only ~1% and 0.2% were found to brightly fluoresce at D1 and D4, respectively (Fig. 1 *D* and *C*). Despite the ~10-fold decrease in the percentage of parasites

Author contributions: P.G., J.T., S.T., T.I., G.M., R.M., and R.A. designed research; P.G., J.T., S.T., T.I., B.F.-F., C.J.J., and R.A. performed research; F.B., B.F.-F., and C.J.J. contributed new reagents/analytic tools; P.G., J.T., S.T., F.B., T.I., B.F.-F., C.J.J., R.M., and R.A. analyzed data; and R.M. and R.A. wrote the paper.

The authors declare no conflict of interest.

*This Direct Submission article had a prearranged editor.

[1]Present address: Department of Molecular Parasitology, Ehime University Graduate School of Medicine, Shitsukawa, Toon, Ehime 7910-0295, Japan.

[2]To whom correspondence should be addressed. E-mail: rmenard@pasteur.fr.

This article contains supporting information online at www.pnas.org/lookup/suppl/doi:10.1073/pnas.1009346107/-/DCSupplemental.

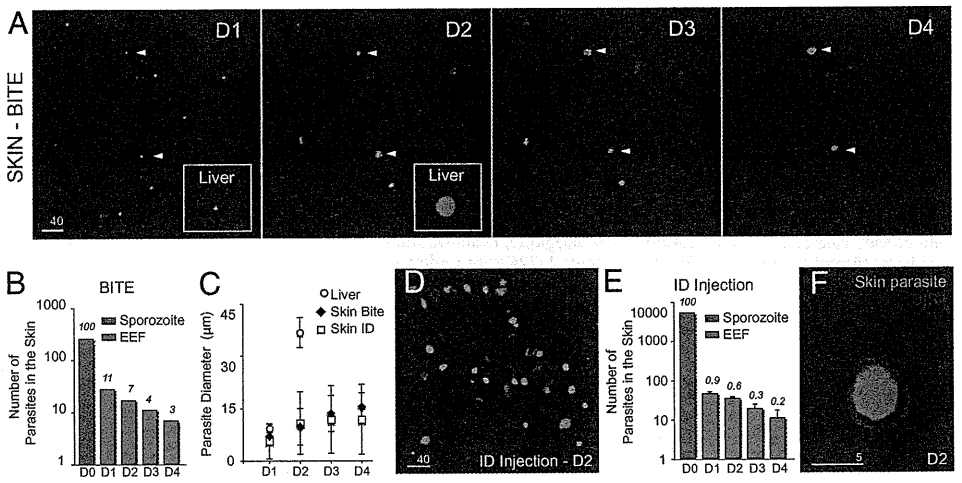

Fig. 1. *P. berghei* differentiation in the ear skin of a *hairless* mouse. (*A*) Parasites (in green) imaged for 4 d (autofluorescence in red) after sporozoite inoculation by the bite of a single mosquito. Images are maximal Z-projections of 13–21 contiguous pictures separated by 5 µm. Red arrowheads, fluorescent parasites fading over time; white arrowheads, brightly fluorescent parasites until day 4 (D4). The lower-right inset shows a liver stage at the same scale at D1 and D2. (Scale bar, 40 µm.) (*B*) Cumulative numbers of developing parasites in six different bite sites from two independent experiments. Orange bar (D0), number of sporozoites detected after the bite (n = 258); green bars, number of brightly fluorescent EEF; numbers above the bars, percentages of developing parasites versus sporozoites imaged at D0. (*C*) Parasite diameter (average ± SD), estimated by the EEF maximum projection area, in the liver (circles) and in the skin (diamond, after bite; square, after injection). (*D*) Parasites (in green) at D2 after microinjection of 5,200 sporozoites. The image is a maximal Z-projection of 35 pictures covering 70 µm in depth. (Scale bar, 40 µm.) (*E*) Numbers of developing parasites after intradermal injection. Orange bar (D0), no. of injected sporozoites (5,200); green bars, numbers of brightly fluorescent EEF (average ± SD), in four injection sites; numbers above the bars, percentages of developing parasites vs. sporozoites injected at D0. Similar results were obtained after injection of larger number of sporozoites (75,000–300,000 parasites). (*F*) Green fluorescent EEF surrounded by a parasitophorous vacuole stained with anti-UIS4 polyclonal antibody (in red) at D2. (Scale bar, 5 µm.)

present at D1 after needle injection compared with mosquito delivery, the fate of surviving parasites was similar in the two cases, as judged by the proportion (Fig. 1 *B* and *E*) and the average size (Fig. 1*C*) of fluorescent EEF.

We then asked whether parasite maturation in the skin occurred within host cells. In hepatocytes, parasites develop inside a parasitophorous vacuole (PV) formed upon sporozoite entry into the host cell (17). The sporozoite transmembrane protein UIS4 inserts into the PV membrane and is essential for liver-stage development (18). Staining of skin cryosections with anti-UIS4 antibodies (Fig. 1*F*) showed that 53% and 65% of the green fluorescent EEF were delineated by a clear red UIS4 signal at D1 and D2, respectively.

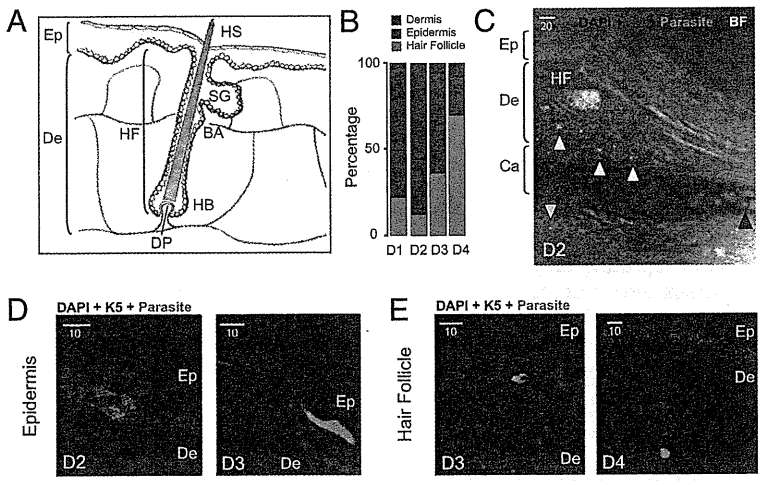

Fig. 2. Localization of *P. berghei* skin EEF. (*A*) Schematic view of the epidermis, dermis, and hair follicle of the mammalian skin. Drawn are the keratin5-positive keratinocytes (in red) that rest on the basement membrane separating the dermis from the epidermis and line the invagination of the HF; the Blimp1-positive cells (in green) associated with the superficial layer of the epidermis and the HF; and the vascularization in the dermis (red lines). Ep, epidermis; De, dermis; HF, hair follicle; HS, hair shaft; SG, sebaceous gland; BA, bulge area; HB, hair bulb; DP, dermal papilla. (*B*) Percentage of dermal (blue), epidermal (red), and hair follicle-associated (green) parasites in the mouse ear estimated by immunofluorescence microscopy at various days after intradermal injection of sporozoites. Number of analyzed EEF for each time point: 33–63. (*C*) Confocal image showing EEF (in green) in the deep dermis (white arrowheads), the epidermis (yellow arrowhead), and the cartilage (red arrowhead). Abbreviations are as in *A*; Ca, cartilage. (Scale bar, 20 µm.) (*D*) Confocal images of epidermal EEF (in green), associated with keratin5-positive keratinocytes of the basal layer of the epidermis (*Left*) or with keratin5-negative keratinocytes of the superficial layers of the epidermis (*Right*). Abbreviations are as in *A*. (Scale bar, 10 µm.) (*E*) Confocal images of hair follicle-associated EEF. EEF (in green) are located in the upper portion of the HF, in keratin5-positive or keratin5-negative cells, often near the sebaceous glands. Abbreviations are as in *A*. (Scale bar, 10 µm.)

We also analyzed the development in the mouse skin of sporozoites lacking the P36p protein. P36p is important for the formation and/or maintenance of the PV membrane, and a *P. berghei P36p* knockout clone generates ~5–10% of the EEF produced by WT sporozoites inside hepatocytes (19, 20). We constructed the *P. berghei* clone P36p-G bearing both the *P36p-* null mutation and a GFP-expression cassette (Fig. S1), and sporozoites of the clone were coinjected with red-fluorescent WT sporozoites of the L733 clone (21) into the skin of mice. Approximately 10-fold fewer green P36p-G than red WT EEF were observed at D1 at the injection site (Fig. S1). Together, these data suggested that most WT *P. berghei* parasites surviving in the mouse skin were developing intracellularly inside a PV.

***P. berghei* Develops in the Epidermis and Dermis and in Association with Hair Follicles.** We next localized the EEF in the skin using an immunohistological approach (see Fig. 2*A* for a schematic representation of the mammalian skin). *P. berghei* sporozoites (2×10^5) were injected into the ear skin of *hairless* mice, and at various days postinoculation ~10-μm cryosections of fixed ear tissues were labeled with DAPI and immunostained using antibody K5, which recognizes keratin5 in keratinocytes of the basal layer of the epidermis (22). EEF were present in multiple sites in the skin. (*i*) At D1 and D2, ~50% of the EEF were located in the dermis (Fig. 2*B* and *C* and Fig. S2*A*). Dermal EEF behaved similarly to liver EEF, with a sharp decrease between D2 and D3, and only represented ~7% of the skin EEF at D3 and D4 (Fig. 2*B*). (*ii*) EEF were also found in the epidermis. At D1 and D2, epidermal EEF were associated mostly with keratin5-positive keratinocytes lying on the basement membrane, whereas at D3 and D4 they were mostly in keratin5-negative cells in the superficial layers of the epidermis (Fig. 2*D* and Fig. S2*B*). The number of epidermal EEF did not significantly change up to D3, and only slightly decreased at D4 (Fig. 3*A*). (*iii*) More surprisingly, EEF were found in close association with hair follicles, appearing as keratin5-positive keratinocyte-bound tubular invaginations of the epidermis (Fig. 2*E* and Fig. S2*C*). In *hairless* mice, EEF associated with the autofluorescent (and rudimentary) hair follicles were frequently located close to the sebaceous glands (Fig. 2*E* and Fig. S2*C*). Their numbers remained stable up to D4 (Fig. 3*A*), representing 70% of the skin EEF at D4 (Fig. 2*B*), and parasites were still detected in hair follicles after more than 2 wk postinoculation (Fig. 3*B*).

Parasite association with hair follicles was also imaged in a Blimp1-GFP mouse (23). In this mouse, a group of cells expressing the transcriptional repressor B lymphocyte-induced maturation protein 1 (Blimp1) and residing near the bud site of the sebaceous glands, which act as sebocyte progenitor cells, are green fluorescent (24). After injection of red fluorescent WT sporozoites into the ear of a Blimp1-GFP mouse, red fluorescent EEF were found associated with the green fluorescent area of hair follicles (Fig. 3*C*, skin). As in the hairless mice, hair follicle-associated EEF were observed persisting for several days, in the vicinity of the GFP-fluorescent zone of the sebaceous glands (Fig. 3*C*, hair follicle). It is still unclear, however, whether these parasites were simply growing slowly in the skin or might include true dormant (growth-arrested) forms.

***P. berghei* Developing in the Mouse Skin Generates Merozoites.** We next imaged parasite growth in the skin using bioluminescence. For this, we used sporozoites of the transgenic *P. berghei* clone 676cl1 (Pb*GFP-LUC*$_{SCH}$) expressing a GFP-luciferase fusion gene via the *EEF1α* promoter (25), which constitutively produces the fusion protein throughout the parasite life cycle. Sporozoites (2×10^4) were inoculated in the ear skin of mice and luciferin injected immediately before real-time whole-body imaging of mice using the IVIS system (26). Bioluminescent signals were detected only in the ear and the liver at D2 (Fig. S3). The main signal was detected in the liver, peaking at D2, and the signal in the ear skin peaked at D3.

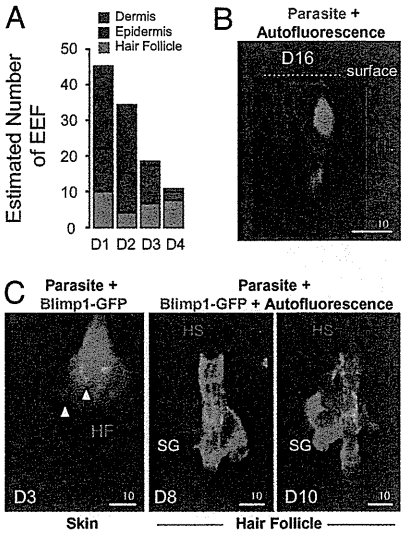

Fig. 3. *P. berghei* association with hair follicles. (*A*) Numbers of dermal, epidermal, and hair follicle-associated EEF after intradermal injection of sporozoites, obtained by multiplying the numbers of skin EEF counted by intravital microscopy (Fig. 1*E*) by the percentages of dermal, epidermal, and hair follicle-associated parasites counted by histology (Fig. 2*B*). (*B*) Intravital confocal image showing EEF surviving inside a hair follicle in the ear of a *hairless* mouse at D16 after microinjection of sporozoites. The images are a lateral view of a 3D reconstruction of the skin. Parasites are in green and the hair follicle autofluoresces in red. (Scale bar, 10 μm.) (*C*) Intravital confocal images showing red fluorescent EEF in the ear skin of a Blimp1-GFP mouse. (*Left*) D3: Z-projection of 70 slices covering 35 μm showing red fluorescent EEF inside a hair follicle (white arrowheads). (*Center*) D8 and (*Right*) D10: red EEF in a hair follicle in close association with Blimp1-GFP-positive cells. (Scale bars, 10 μm.)

Quantification of the intensity of bioluminescence signals using the Living Image software showed that the signal in the ear skin increased ~threefold between D1 and D2, and ~2.5-fold between D2 and D3 (Fig. 4*A*). This suggested that, like liver parasites, skin parasites could actively grow.

To investigate schizogony in skin parasites, we examined individual skin EEF at D3 and D4, when most had reached their maximal size, by confocal microscopy. In *hairless* mice, fluorescent parasites were seen undergoing nuclear divisions (Fig. S4) and generating individual merozoite-like progeny (Fig. 4*B*). Further, infected cells in the skin were frequently observed giving rise to cell extensions reminiscent of the merosomes that extrude from infected hepatocytes (Fig. S5*A*). Hepatocyte-derived merosomes contain tens to thousands of merozoites wrapped in the host cell membrane, bud off, and detach from the infected cell to reach the blood in the liver sinusoids (27). Brightly fluorescent merosome-like extensions were also observed detaching from infected cells (Fig. 4*C*) and moving in the skin (Fig. 4*C* and Fig. S5*B*).

To test whether the fluorescent progeny seen inside skin cells were indeed merozoites, we tested their capacity to invade and multiply in mouse erythrocytes. One day after injection of green fluorescent sporozoites into the skin of mice ($1.0–2.5 \times 10^5$ sporozoites per ear in 2–4 animals), i.e., before the first merozoites are formed in the liver, the skin tissue at the injection site was dissected and treated with collagenase and trypsin to obtain a single cell suspension. Infected fluorescent cells were sorted by FACS (Fig. 5*A*) and incubated for several days at 37 °C in vitro in DMEM 10% FCS. Examination of the sorted cells confirmed the diversity of skin cell types that were infected in situ (Fig. 5*B*), and after 4 d (1 d in the skin and 3 d in vitro), merozoites were detected inside sorted cells (Fig. 5*C*). At D4, cells were scratched and the host cell/

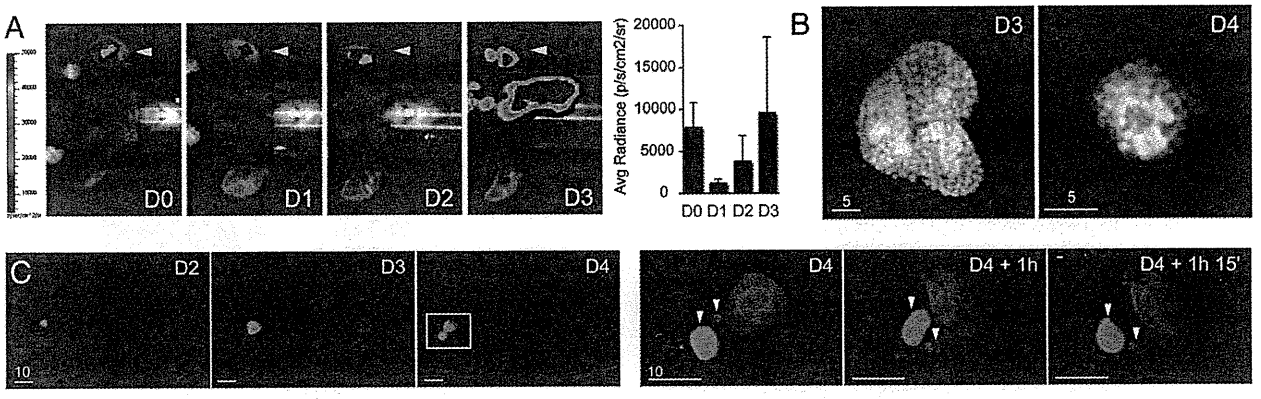

Fig. 4. *P. berghei* complete development inside skin cells. (*A*) Parasite development in the skin measured by bioluminescence. The 2×10^4 GFP::LUC sporozoites were microinjected in the ear of C57BL6 mice (yellow arrowhead) and recorded from D0 to D3 following injection of luciferin. The graph represents the difference between the average radiance of the inoculated ear and the contralateral ear at D0, 1, 2, and 3 (mean ± SD; $n = 3$). (*B*) Mature schizonts in the skin. Intravital imaging of merozoite-filled EEF in the ears of mice at D3 and D4. (Scale bars, 5 μm.) (*C*) Skin EEF release merosomes. (*Left*) Skin EEF growing and budding between D3 and D4 after mosquito bite. (*Right*) Time-lapse recording of the squared area depicted at D4 and shows the release and movement of fluorescent structures of various sizes. White arrowheads, merosomes; red arrowheads, merozoites. (Scale bars, 10 μm.)

parasite mixture injected i.v. into mice. In three independent experiments (Fig. 5*D*), mice became infected and parasitemia increased at a normal rate (~10-fold increase/24 h). This demonstrates that *P. berghei* development in skin cells can generate infective merozoites, and thus that the parasite developmental pathway in the skin indeed reproduced that in the liver.

In Situ Infectivity of *P. berghei* Merozoites Generated in Skin Cells. To test whether merozoites generated in skin cells (skin-derived merozoites) were capable of invading erythrocytes in situ and sufficient for generating a blood stage infection, transplantation experiments of infected skins onto naive mice were complicated by the different timings of maximal release of skin-derived merozoites (D2–D3 post-sporozoite inoculation) and of efficient vascularization of the skin graft. Strikingly, we observed that primaquine, a drug known to inhibit liver EEF development, had a much weaker effect on skin EEF development (Fig. S6*A*). After injection of luciferase-producing sporozoites in the ear of mice, treatment with 25 mg/kg primaquine at D0 and D1 abolished the bioluminescence signal in the liver without affecting that in the ear. However, this differential primaquine effect could not be exploited to show the in vivo infectivity of skin-derived merozoites. Indeed, the 25-mg/kg primaquine treatment did not completely prevent liver EEF maturation in all animals (5 of 52 primaquine-treated mice and surgically deprived of the infected ear at D1 became patent; see Fig. S7) and impaired skin EEF development between D2 and D3 (Fig. S6*A*), whereas 30 mg/kg primaquine significantly affected skin EEF development at earlier time points (Fig. S6*A*).

In any case, the skin-derived merozoites are clearly outnumbered by their liver-derived counterparts, and their contribution to the onset of blood stage infection would be minimal at best. After injection of luciferase-producing sporozoites in the skin of mice, the maximal intensity signal at the injection site, reached at D3, was found to be ~2% of the maximal intensity signal in the liver, reached at D2 (Fig. S6*B*). Not surprisingly, when sporozoites were injected in the ear of mice and the infected or controlateral ear was surgically removed at D1, no statistical difference was detected in the parasitemia of animals lacking or having skin EEF (Fig. S6*C*).

***P. yoelii* Generates Merozoites in the Mouse Skin.** Last, we studied the development of sporozoites of *Plasmodium yoelii*, another species that infects rodents, in the mouse skin. Like sporozoites of *P. falciparum*, the species most lethal to humans, *P. yoelii* sporozoites are known to invade only certain hepatocytic lines in vitro, in a CD81-dependent manner (28). Additionally, quantitative PCR analysis of mouse ear inoculated with *P. yoelii* sporozoites showed that the parasite DNA was still detected 42 h postinjection in the mouse skin (13). We analyzed the fate of *P. yoelii* sporozoites expressing GFP (29) or RedStar (Fig. S8) after intradermal injection in mice. At D1, ~0.2% and ~0.15% of the inoculated sporozoites transformed in the ear skin of *hairless* and Swiss mice, respectively (Fig. S9*A*). Despite the ~fivefold smaller

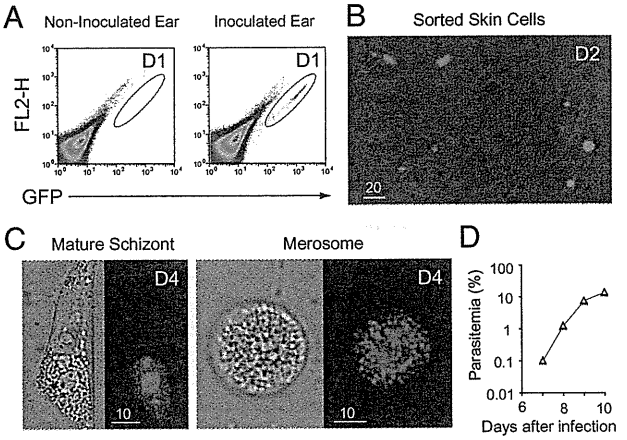

Fig. 5. Merozoite production by and in vivo infectivity of *P. berghei* skin EEF. (*A*) Sorting of infected skin cells. The 1.0–2.5 × 10^5 sporozoites were microinjected in the ear of C57BL6 mice. The pseudocolor plot shows the distribution of skin cells obtained from the ears of noninfected (*Left*) and infected mice (*Right*) 1 d postinfection. The green oval represents the gate used for sorting the infected skin cells, which were collected in 96-wells cell culture plate and kept at 37 °C, 5% CO_2 in DMEM 10% FCS. No events were detected using the noninfected ear. (*B*) Wide-field microscopy of sorted cells showing the variety of infected skin cell types (bright field and green) at D2—1 d in the skin and 1 d in vitro. (Scale bar, 20 μm.) (*C*) Generation of merozoites within skin cells. Presence of merozoites inside an adherent skin cell (*Left*) and in a floating merosome (*Right*). (Scale bar, 10 μm.) (*D*) A representative parasitemia curve following injection of merozoite-filled skin cells at D4—1 d in the skin and 3 d cultured in vitro. The number of events sorted at D1 in this experiment was 1,200 (~600 GFP^+ cells), resulting in approximately four mature schizonts after 3 d in culture. The parasitemia was accessed by FACS and blood smear.

number of *P. yoelii* parasites observed in the skin compared with *P. berghei* at D1, *P. yoelii* EEF, like *P. berghei* EEF, grew both in the epidermis and the dermis of mice (Fig. S9*B*). *P. yoelii* merozoites were detected from D2 onward (Fig. S9*C*) and were seen moving across the skin (Fig. S9*D*), indicating that *P. yoelii* EEF completed their development in the skin of mice.

Conclusions

This study shows that the *P. berghei* and *P. yoelii* rodent-infecting species can undergo complete exoerythrocytic schizogony not just inside hepatocytes but also inside skin cells. However, although the *P. berghei* infective merozoites released and moving in the skin in merosome-like extensions might occasionally invade erythrocytes in the mouse, and thus constitute a potential secondary reservoir of infective merozoites, skin-derived merozoites do not significantly contribute to erythrocyte infection in normal conditions. Whether other mammal-infecting *Plasmodium* species, particularly the human-infecting species, can also develop in the skin of the host remains to be addressed.

The data also suggest that parasites might persist in association with hair follicles, which constitute an immunoprivileged site of the mammalian body characterized by the virtual absence of major histocompatibility complex (MHC) class I expression and a strongly immunosuppressive environment (30). This raises the hypothesis that parasites might become quiescent when associated with hair follicles and act as a source of infection relapses, as proposed for the hypnozoites of *P. vivax* in the liver (31).

Perhaps the most important implication of this work is immunological. Whereas previous data (11, 12) showed that in the mouse ear model about half of the *P. berghei* sporozoites inoculated by mosquitoes stayed at the bite site, the present data indicate that ~10% of the injected sporozoites are developing at D1 in the skin. This implies that the lymph node that drains the injection site will receive parasite antigens not just from sporozoites (sporozoites actively reaching the lymph node or dead sporozoites left in the skin) but also from differentiating parasites (skin EEF aborting at various stages of their development). Overall, in the *P. berghei*/ear skin model system, the draining lymph node receives up to 70% of the parasite antigens inoculated by mosquito bite. The tolerogenic or protective properties of the various kinds of skin-derived parasite antigens will have to be assessed, in natural as well as immunizing conditions. This would be particularly important in the case of live attenuated (irradiated or genetically modified) sporozoites, which have been known for many years to act as powerful vaccines in animal models (32) and will soon undergo human trials (33–35), because in humans they can only be inoculated in the skin.

Materials and Methods

Parasites, Mice, and Mosquitoes. We used the *P. berghei* ANKA clone expressing GFP under the control of the *hsp70* promoter (14). The *P. yoelii* GFP-expressing parasite clone was obtained from the MR4 repository (ATCC no. MRA-817; 17XNL PYGFP). The red fluorescent *P. berghei* line (line 733) contains the RedStar-expressing cassette integrated at the *230p* genomic locus. The red fluorescent *P. yoelii* clone contains the RedStar cassette integrated at the *d-ssu-rrna* locus. We used the *P. berghei* clone 676cl1 (Pb*GFP-LUC*$_{SCH}$) expressing a GFP-luciferase fusion gene via the *EEF1α* promoter (25). C57BL/6, Swiss and *hairless* SKH1 mice were purchased from Charles River Laboratories. All experiments were approved by the committee of Institut Pasteur and were performed in accordance with the applicable guidelines and regulations. *A. stephensi* (Sda500 strain) mosquitoes were reared using standard procedures (16). For intradermal injection of sporozoites into rodents, salivary gland sporozoites were dissected out and a small volume (0.2–10 μL) containing 5×10^3 to 3×10^5sporozoites was deposited in the dermis of the ear by using a 35- to 36-gauge needle with a NanoFil syringe (World Precision Instruments).

Intravital Imaging and Immunolabelings. Intravital imaging was performed as described (16). For immunolabelings, ears were excised, fixed with 4% paraformaldehyde/PBS for 2 h, and dehydrated in 10% and 30% sucrose/PBS before embedding in OCT. Ten-micrometer sections were cut on a CM3050S cryostat (Leica) and adhered to Superfrost Plus Slides (VWR). Sections were permeabilized and blocked in PBS containing 0.1% Triton X-100 (Sigma) and 5% FCS, followed by staining with anti-keratin5 polyclonal primary antibody (Covance) or anti-UIS4 polyclonal primary antibody, AlexaFluor 546 conjugate (Molecular Probes), and DAPI (Molecular Probes). Stained slides were mounted with Prolong Gold (Invitrogen), and 3D image stacks were acquired on a SP5 confocal microscope (Leica). Images are displayed as 2D maximum-intensity projections.

ACKNOWLEDGMENTS. We thank Stéphane Vincent (Institut Pasteur) and Mitinori Saitou (Riken Center for Developmental Biology) for the kind gift of Blimp1-GFP mice. We thank Spencer Shorte, Marie Nguyen-de Bernon, and Marie-Anne Nicola and the Imagopole team (Institut Pasteur) for help with microscopy, cytometry, and bioluminescence; Catherine Bourgouin, Isabelle Thiéry and the other members of the CEPIA platform (Institut Pasteur) for rearing mosquitoes; Masao Yuda (Mie University) for the gift of anti-HSP70 antibodies; Stephan Kappe (Seattle Biomedical Research Institute) for the gift of anti-UIS4 antibodies; and Jean-Jacques Panthier and Geneviève Aubin-Houzelstein (Institut Pasteur) for helpful discussions. We acknowledge funding from Fundação para a Ciência e Tecnologia Grant SFRH/BPD/48340/2008 (to J.T.) and Institut Pasteur, Natixis, the BioMalPar European Network of Excellence, the Agence Nationale pour la Recherche, and the Howard Hughes Medical Institute (to R.M.).

1. Huff CG (1947) Life cycle of malarial parasites. *Annu Rev Microbiol* 1:43–60.
2. Shortt HE, Garnham PC (1948) Pre-erythrocytic stage in mammalian malaria parasites. *Nature* 161:126.
3. Vanderberg JP (1981) *Plasmodium berghei* exoerythrocytic forms develop only in the liver. *Trans R Soc Trop Med Hyg* 75:904–905.
4. Meis JF, Verhave JP (1988) Exoerythrocytic development of malarial parasites. *Adv Parasitol* 27:1–61.
5. Shortt HE, Garnham PC (1948) Demonstration of a persisting exo-erythrocytic cycle in *Plasmodium cynomolgi* and its bearing on the production of relapses. *BMJ* 1: 1225–1228.
6. Krotoski WA, et al. (1982) Demonstration of hypnozoites in sporozoite-transmitted *Plasmodium vivax* infection. *Am J Trop Med Hyg* 31:1291–1293.
7. Shortt HE, Fairley NH, Covell G, Shute PG, Garnham PC (1951) The pre-erythrocytic stage of *Plasmodium falciparum*. *Trans R Soc Trop Med Hyg* 44:405–419.
8. Yoeli M, Vanderberg JP, Upmanis RS, Most H (1965) Primary tissue phase of *Plasmodium berghei* in different experimental hosts. *Nature* 208:903.
9. Sidjanski S, Vanderberg JP (1997) Delayed migration of *Plasmodium* sporozoites from the mosquito bite site to the blood. *Am J Trop Med Hyg* 57:426–429.
10. Vanderberg JP, Frevert U (2004) Intravital microscopy demonstrating antibody-mediated immobilisation of *Plasmodium berghei* sporozoites injected into skin by mosquitoes. *Int J Parasitol* 34:991–996.
11. Amino R, et al. (2006) Quantitative imaging of *Plasmodium* transmission from mosquito to mammal. *Nat Med* 12:220–224.
12. Kebaier C, Voza T, Vanderberg JP (2009) Kinetics of mosquito-injected *Plasmodium* sporozoites in mice: Fewer sporozoites are injected into sporozoite-immunized mice. *PLoS Pathog* 5:e1000399.
13. Yamauchi LM, Coppi A, Snounou G, Sinnis P (2007) *Plasmodium* sporozoites trickle out of the injection site. *Cell Microbiol* 9:1215–1222.
14. Ishino T, Orito Y, Chinzei Y, Yuda M (2006) A calcium-dependent protein kinase regulates *Plasmodium* ookinete access to the midgut epithelial cell. *Mol Microbiol* 59: 1175–1184.
15. Panteleyev AA, et al. (1998) Towards defining the pathogenesis of the hairless phenotype. *J Invest Dermatol* 110:902–907.
16. Amino R, et al. (2007) Imaging malaria sporozoites in the dermis of the mammalian host. *Nat Protoc* 2:1705–1712.
17. Baldacci P, Ménard R (2004) The elusive malaria sporozoite in the mammalian host. *Mol Microbiol* 54:298–306.
18. Mueller AK, et al. (2005) *Plasmodium* liver stage developmental arrest by depletion of a protein at the parasite-host interface. *Proc Natl Acad Sci USA* 102:3022–3027.
19. Ishino T, Chinzei Y, Yuda M (2005) Two proteins with 6-cys motifs are required for malarial parasites to commit to infection of the hepatocyte. *Mol Microbiol* 58: 1264–1275.
20. van Dijk MR, et al. (2005) Genetically attenuated, P36p-deficient malarial sporozoites induce protective immunity and apoptosis of infected liver cells. *Proc Natl Acad Sci USA* 102:12194–12199.
21. Sturm A, et al. (2009) Alteration of the parasite plasma membrane and the parasitophorous vacuole membrane during exo-erythrocytic development of malaria parasites. *Protist* 160:51–63.
22. Dai X, Segre JA (2004) Transcriptional control of epidermal specification and differentiation. *Curr Opin Genet Dev* 14:485–491.
23. Ohinata Y, et al. (2005) Blimp1 is a critical determinant of the germ cell lineage in mice. *Nature* 436:207–213.

24. Horsley V, et al. (2006) Blimp1 defines a progenitor population that governs cellular input to the sebaceous gland. *Cell* 126:597–609.
25. Franke-Fayard B, et al. (2008) Simple and sensitive antimalarial drug screening in vitro and in vivo using transgenic luciferase expressing *Plasmodium berghei* parasites. *Int J Parasitol* 38:1651–1662.
26. Franke-Fayard B, Waters AP, Janse CJ (2006) Real-time in vivo imaging of transgenic bioluminescent blood stages of rodent malaria parasites in mice. *Nat Protoc* 1: 476–485.
27. Sturm A, et al. (2006) Manipulation of host hepatocytes by the malaria parasite for delivery into liver sinusoids. *Science* 313:1287–1290.
28. Silvie O, et al. (2003) Hepatocyte CD81 is required for *Plasmodium falciparum* and *Plasmodium yoelii* sporozoite infectivity. *Nat Med* 9:93–96.
29. Ono T, Tadakuma T, Rodriguez A (2007) *Plasmodium yoelii yoelii* 17XNL constitutively expressing GFP throughout the life cycle. *Exp Parasitol* 115:310–313.
30. Mellor AL, Munn DH (2006) Immune privilege: A recurrent theme in immunoregulation? *Immunol Rev* 213:5–11.
31. Cogswell FB (1992) The hypnozoite and relapse in primate malaria. *Clin Microbiol Rev* 5:26–35.
32. Mulligan HW, Russell PF, Mohan BN (1941) Active immunization of fowls against *Plasmodium gallinaceum* by injections of killed homologous sporozoites. *J Malaria Inst India* 4:25–34.
33. Luke TC, Hoffman SL (2003) Rationale and plans for developing a non-replicating, metabolically active, radiation-attenuated *Plasmodium falciparum* sporozoite vaccine. *J Exp Biol* 206:3803–3808.
34. Matuschewski K (2006) Vaccine development against malaria. *Curr Opin Immunol* 18: 449–457.
35. Mikolajczak SA, Aly AS, Kappe SH (2007) Preerythrocytic malaria vaccine development. *Curr Opin Infect Dis* 20:461–466.

INFECTION AND IMMUNITY, Sept. 2010, p. 3773–3782
0019-9567/10/$12.00 doi:10.1128/IAI.00306-10

Vol. 78, No. 9

Plasmodium vivax Ookinete Surface Protein Pvs25 Linked to Cholera Toxin B Subunit Induces Potent Transmission-Blocking Immunity by Intranasal as Well as Subcutaneous Immunization▽

Takeshi Miyata,[1] Tetsuya Harakuni,[1] Takafumi Tsuboi,[2] Jetsumon Sattabongkot,[3] Hideyasu Kohama,[1]† Mayumi Tachibana,[4] Goro Matsuzaki,[1,5] Motomi Torii,[4] and Takeshi Arakawa[1,5]*

Molecular Microbiology Group, Department of Tropical Infectious Diseases, COMB, Tropical Biosphere Research Center, University of the Ryukyus, 1 Senbaru, Nishihara, Okinawa 903-0213, Japan[1]; Cell-Free Science and Technology Research Center, Ehime University, Matsuyama, Ehime 790-8577, Japan[2]; Department of Entomology, Armed Forces Research Institute of Medical Sciences, Bangkok 10400, Thailand[3]; Department of Molecular Parasitology, Ehime University Graduate School of Medicine, Shitsukawa, Toon, Ehime 791-0295, Japan[4]; and Division of Host Defense and Vaccinology, Graduate School of Medicine, University of the Ryukyus, 207 Uehara, Nishihara, Okinawa 903-0213, Japan[5]

Received 26 March 2010/Returned for modification 20 April 2010/Accepted 16 June 2010

The nontoxic cholera toxin B subunit (CTB) was evaluated as a potential delivery molecule for the *Plasmodium vivax* ookinete surface protein, Pvs25. Recombinant Pvs25 was expressed as a secreted protein in the yeast *Pichia pastoris*, as a mixture of isoforms including multimers and the A and B monomers. The A isoform with the presumed native protein fold was the most abundant, accounting for more than 40% of all expressed protein. The molecularly uniform A isoform was chemically conjugated to CTB via its primary amines, and the fusion protein, retaining GM1-ganglioside affinity, was administered to BALB/c mice by the subcutaneous (s.c.) or intranasal (i.n.) route. Immunization of mice with conjugated Pvs25 without supplemental adjuvant induced antisera that specifically recognized *P. vivax* ookinetes *in vitro*. Furthermore, the antisera, when mixed with parasitized blood isolated from *P. vivax* patients from Thailand, was found to reduce parasite transmission to mosquitoes, conferring a 93 to 98% (s.c.) or a 73 to 88% (i.n.) decrease in oocyst number. Unconjugated Pvs25 alone conferred only a 23 to 60% (s.c.) or a 0 to 6% (i.n.) decrease in oocyst number. Coadministration of extraneous adjuvants, however, further enhanced the vaccine efficacy up to complete blockade. Taken together, we conclude that a weakly immunogenic Pvs25 by itself, when linked to CTB, transforms into a potent transmission-blocking antigen in both i.n. and s.c. routes. In addition, the present study is, to the best of our knowledge, the first demonstration of the immune potentiating function of CTB for a vaccine antigen delivered by the s.c. route.

Malaria is one of the most serious infectious diseases, with high mortality and morbidity, especially in tropical regions of the world. The disease causes 350 to 500 million clinical cases every year, and the estimated annual mortality exceeds 1.1 million (28). Implementation of many malaria control measures, including chemotherapy and insecticide-treated bed nets, have made a significant contribution to the reduction of malaria cases worldwide; however, these control measures are suboptimal, and hence new tools, particularly vaccines, should be used for local elimination and the ultimate eradication of malaria from the globe (9, 10, 24). The development of effective and affordable malaria vaccines is therefore likely to benefit global public health (Malaria Vaccine Technology Roadmap [MVTR], 2006 [http://www.malariavaccineroadmap.net/pdfs/Malaria_Vaccine_TRM_Final.pdf]).

Although *Plasmodium falciparum* causes the highest mortality rates among the four *Plasmodium* species known to infect humans (18), *P. vivax* malaria has the highest morbidity and is an important cause of recurrent malaria. This species is therefore an important target of malaria control efforts (4–6; MVTR). Furthermore, because global malaria eradiation is the ultimate goal, the value of developing vaccines against *P. vivax* cannot be underestimated (4–6; MVTR). Several promising vaccine candidates have been intensively investigated, such as those targeting the asexual stages, i.e., the sporozoite, hepatic and erythrocytic stages, which are designed to prevent infection and to reduce disease severity. On the other hand, transmission-blocking vaccines (TBVs) that target the sexual stage, in which the parasite undergoes sporogonic development in anopheline mosquitoes, prevent parasite transmission from mosquitoes to humans (7, 14, 25). TBVs induce antibodies that react with the ookinete surface proteins (OSPs) of malaria parasites within the mosquito midgut, and as such they do not directly protect vaccinated individuals from infection. They could, however, contribute to elimination of the disease by lowering the parasite transmission frequency below the threshold at which the parasite can maintain its life cycle (4, 6). In addition, TBVs, when combined with vaccines targeting other stages of the infection, could prevent transmission of parasites that have escaped the immune response. Furthermore, TBVs could also prevent transmission of drug-resistant

* Corresponding author. Mailing address: Molecular Microbiology Group, Department of Tropical Infectious Diseases, COMB, Tropical Biosphere Research Center, University of the Ryukyus, 1 Senbaru, Nishihara, Okinawa 903-0213, Japan. Phone and fax: 81-98-895-8974. E-mail: tarakawa@comb.u-ryukyu.ac.jp.

† Present address: Japan BCG Laboratory, 3-1-5 Matsuyama, Kiyose, Tokyo 204-0022, Japan.

▽ Published ahead of print on 28 June 2010.

parasites, which will likely to emerge when mass administration of primaquine is initiated. Therefore, TBVs might function as a "safety net" for pre-erythrocytic and erythrocytic vaccines, as well as other nonvaccine interventions.

We have recently tested whether a mucosal vaccination regime can be applied to TBVs, on the premise that noninvasive and easy-to-administer mucosal vaccines are advantageous in a mass vaccination campaign in a region where malaria is endemic (1–3). In these animal studies, we have demonstrated the potential of mucosal vaccines to block parasite transmission, but enhancement of the mucosal immunogenicity of recombinant antigens was found to be critically dependent upon the use of cholera toxin (CT) adjuvant. CT is well known for its high immune potentiating function for admixed antigens administered through the mucosal, particularly the intranasal (i.n.), route (13). However, its clinical application is hampered by its severe toxicity (26). Thus, alternative vaccine formulations not using the CT holotoxin are highly desirable.

Here, we extended our previous studies to test our hypothesis that the immunogenicity of a *Plasmodium vivax* malaria OSP, Pvs25, becomes substantially augmented when physically linked to the nontoxic B subunit of CT (CTB), even without supplementation with extraneous adjuvants. This should, in theory, effectively reduce parasite transmission to mosquitoes. Furthermore, we tested the TBV efficacy of the engineered fusion complex in a subcutaneous (s.c.) immunization regimen to test the immune potentiating function of CTB with this particular immunization route.

MATERIALS AND METHODS

Expression of Pvs25H protein from the methylotrophic yeast *Pichia pastoris*. The Pvs25 coding region (Ala_{23} to Leu_{195}) was amplified by PCR from plasmid Pvs25#26_SalI_pEU3, which harbors the coding region for the extracellular domain of the Pvs25 protein (12), with a sense primer (5′-GCCGTCACGGTA GACACC-3′) and an antisense primer containing an EcoRI site, a hexahistidine-coding sequence and a termination codon (5′-GGGAATTCTTAATGATGGT GATGGTGATGTGGTCCAAGGCATACATTTTTCTCTTTGTC-3′). The DNA fragment was amplified by using *Vent* DNA polymerase (New England Biolabs, Beverly, MA), was purified by using a PCR Purification Kit (Qiagen, Inc., Valencia, CA), and then digested with EcoRI. The fragment was subcloned into the SnaBI and EcoRI sites of the *P. pastoris* expression vector pPIC9K (Life Technologies, Carlsbad, CA) to construct the plasmid pPvs25H, which was designed to express an α-factor signal–Pvs25–hexahistidine fusion protein (see Fig. 1a).

P. pastoris recombination was performed according to the manufacturer's instructions (Life Technologies). Approximately 10 μg of linearized pPvs25H plasmid digested with SalI was electroporated into *P. pastoris* strain GS115 by using a Gene Pulser (1.5 kV, 200 Ω, 25 μF; Bio-Rad Laboratories, Inc., Redmond, WA). Immediately after electroporation, the cells were plated on minimal dextrose medium and incubated for 72 h at 29°C. Colonies were transferred to yeast extract-peptone-dextrose (YPD) medium containing increasing concentrations of Geneticin (G418; 1 to 5 mg/ml; Nacalai Tesque, Inc., Kyoto, Japan) for the selection of clones containing multiple copies of the desired gene. Clones that acquired a phenotype resistant to the highest level of G418 (5 mg/ml) were analyzed for production of the Pvs25H protein. Selected clones were cultured in BMGY medium with vigorous shaking in a baffled flask at 30°C until the optical density at 600 nm (OD_{600}) reached 2.0; the cultured cells were then transferred to BMMY medium containing 0.5% methanol to induce gene expression. Cells were cultured for an additional 72 h, with supplementation with 0.5% methanol for every 24 h of continued induction. The culture supernatant was collected by two rounds of centrifugation (9,600 × *g*) for 10 min, followed by filtration (FastCap filter with a 0.2-μm pore size; Nalgene Nunc International, Inc., Rochester, NY) to remove residual cells completely. Proteins secreted into the supernatant were separated by sodium dodecyl sulfate polyacrylamide gel electrophoresis (SDS-PAGE) and stained with Coomassie brilliant blue or subjected to immunoblot analysis with anti-Pvs25 antiserum or anti-histidine tag monoclonal antibody (Roche, Basel, Switzerland). The supernatant was supplemented with 20 mM imidazole and applied to an immobilized metal ion affinity chromatography column (HisTrap FF Ni Sepharose 6 Fast Flow; GE Healthcare, Little Chalfont, United Kingdom). After a washing step with a buffer containing 20 mM imidazole, the Pvs25H protein was eluted with phosphate-buffered saline (PBS) containing 500 mM imidazole. The affinity-purified protein was used for size exclusion chromatography with a flow rate of 0.2 ml/min (HiLoad 16/60 Superdex 75-pg column; GE Healthcare) to separate the monomeric from the multimeric isoforms. The monomeric isoforms that were a mixture of A and B isoforms were then subjected to hydrophobic interaction chromatography (HIC; HiTrap Phenyl Sepharose HP; GE Healthcare), in which both the A and the B isoforms bound to the hydrophobic ligand by adjusting the concentration of ammonium sulfate in the solution to 2 M. Then, a two-step elution process was performed, using 1 M ammonium sulfate for elution of the A isoform, followed by PBS elution of the B isoform.

This highly purified A isoform (Pvs25H-A) was used for all immunization experiments. The endotoxin content of the Pvs25H-A protein was measured by the *Limulus* amebocyte lysate test (Pyrogent Single Test Vials; Cambrex, East Rutherford, NJ), and the endotoxin content was found to be <0.05 endotoxin unit (EU)/μg of protein.

Immobilized *tris*[2-carboxyethyl]phosphine hydrochloride on a beaded agarose support (TCEP; Pierce, Rockford, IL) was used to generate a reduced form of the sulfhydryl groups for recombinant protein samples. In addition, 5,5′-dithio-*bis*-(2-nitrobenzoic acid) (Ellman's reagent; Pierce) and a cysteine hydrochloride monohydrate standard were used to estimate the amounts of free sulfhydryls.

The N-terminal protein sequences were analyzed by the Edman degradation method as described elsewhere, using a protein sequencer (Shimadzu, Kyoto, Japan).

All recombinant DNA experiments were conducted according to the Safety Guidelines for Gene Manipulation Experiments of the University of the Ryukyus.

Chemical conjugation between Pvs25H-A and CTB. Recombinant CTB was expressed and purified as described previously (11), and purified Pvs25H-A was chemically conjugated to CTB by using the heterobifunctional cross-linker *N*-succinimidyl 3-(2-pyridyldithio) propionate (SPDP; Thermo Scientific, Inc., Rockford, IL). One milligram of Pvs25H-A (2 mg/ml in PBS-EDTA) was incubated with SPDP (0.6 mM, final concentration) for 1 h at room temperature to add pyridyl disulfide groups to the primary amines of the protein. The reaction mixture was then desalted and buffer exchanged to PBS by a size exclusion membrane filter (Amicon Ultra-15, MWCO 10,000; Millipore, Billerica, MA) to remove excess reagent and by-products (pyridine 2-thione). Similarly, 1 mg of CTB (2 mg/ml in PBS-EDTA) was incubated with SPDP (0.6 mM, final concentration) for 1 h at room temperature and then desalted and buffer exchanged to PBS. Pyridyldithiol-activated CTB was then incubated with dithiothreitol (DTT; 50 mM, final) for 30 min at room temperature to expose the sulfhydryl groups and then desalted and buffer exchanged to PBS as before. Finally, equal amounts of pyridyldithiol-activated Pvs25H-A and sulfhydryl-activated CTB were mixed, followed by incubation at room temperature overnight for conjugation. The conjugated sample was desalted as before, and the endotoxin content was measured to confirm that there had been no significant contamination during the conjugation process.

To evaluate the conjugation efficiency, untreated Pvs25H-A was separately incubated either with untreated CTB or pyridyldithiol-activated CTB (CTB^{SPDP}). Similarly, pyridyldithiol-activated Pvs25H-A ($Pvs25H\text{-}A^{SPDP}$) was separately incubated with either untreated or DTT-treated CTB (CTB^{DTT} or $CTB^{SPDP/DTT}$, respectively) (see Results and Fig. 2a for details). Each conjugation sample was analyzed by GM1–enzyme-linked immunosorbent assay (GM1-ELISA) as described previously (11). Briefly, 5 μg of monosialoganglioside GM1 (Sigma-Aldrich, St. Louis, MO)/ml, a receptor for CT, diluted with bicarbonate buffer (15 mM Na_2CO_3, 35 mM $NaHCO_3$ [pH 9.6]; 50 μl/well) was coated onto a 96-well microtiter plate (Sumitomo Bakelite Co., Ltd., Tokyo, Japan), and the plate was incubated at 4°C overnight. After washing the plate twice with PBS containing 0.05% Tween 20 (PBS-T) and once with PBS, the plate was blocked with PBS containing 10% skim milk for 2 h at 37°C. Each conjugation sample (2 μg of total protein/well) was then applied to the wells, and the plate was incubated for 2 h at 37°C, followed by incubation with rabbit anti-CT antiserum (1/4,000; Sigma-Aldrich) or mouse anti-Pvs25 antiserum (1/500) for 2 h at 37°C. This was followed by the addition of anti-rabbit or anti-mouse IgG conjugated to alkaline phosphatase (1/4,000; Sigma-Aldrich). Finally, *p*-nitrophenylphosphate (Bio-Rad) was added, and the plate was incubated for 20 min at 37°C. The OD_{415} was measured by using a microplate reader (Bio-Rad).

To evaluate the conjugation state of the fusion complex, 1 mg of conjugation sample was subjected to size exclusion chromatography (HiLoad 16/60 Superdex

75-pg column; GE Healthcare). Molecular weight standards (Gel Filtration Calibration kits LMW; GE Healthcare) were used to estimate the molecular weights of CTB, Pvs25H-A, and their fusion complex by calculating the partition coefficient (K_{av}) values for each protein standard and sample protein.

Immunization with CTB-Pvs25H-A fusion protein and analysis of induced antibodies. Eight-week-old female BALB/c mice were purchased from Japan SLC (Shizuoka, Japan). Mice (four or eight mice per group) were immunized via the s.c. or the i.n. route with 30 μg of Pvs25H-A, a mixture of CTB and Pvs25H-A (30 μg each) or 60 μg of CTB-Pvs25H-A fusion protein. Where indicated, incomplete Freund's adjuvant (IFA; Difco Laboratories, Detroit, MI) or 0.1 to 1.0 μg of CT (List Biological Laboratories, Campbell, CA) was used for s.c. or i.n. adjuvants, respectively. The mice were immunized three times, at weeks 0, 2, and 3.

Mice were anesthetized 1 week after the third immunization (week 4) by intraperitoneal injection of pentobarbital sodium salt (Nacalai Tesque, Inc.) and were sacrificed by exsanguination to collect serum. For specific serum antibody analysis, ELISA plates (Sumilon; Sumitomo Bakelite Co.) were coated with Pvs25H-A (5 μg/ml) in bicarbonate buffer by incubating the plate at 4°C overnight. The plate was washed twice with PBS-T and once with PBS. The plate was blocked with 1% bovine serum albumin (BSA) in PBS for 2 h at 37°C. Twofold serial dilutions of the antisera starting with 50-fold dilution with 0.5% BSA in PBS were applied to the wells in duplicate, which were then incubated for 2 h at 37°C. The plate was then incubated with anti-mouse IgG conjugated to alkaline phosphatase (1/4,000; Sigma-Aldrich) for 2 h at 37°C. *p*-Nitrophenylphosphate (Bio-Rad) was added to the plate for color development, and the absorbance at OD_{415} was measured after 20 min of incubation at 37°C, using a microplate reader (Bio-Rad). The antibody titer was defined as the serum dilution that gave an OD_{415} value equal to 0.1 or as the serum dilution where a one magnitude higher dilution gave an OD_{415} value of <0.1.

All animal experimental protocols were approved by the Institutional Animal Care and Use Committee of the University of the Ryukyus, and the experiments were conducted according to the Ethical Guidelines for Animal Experiments of the University of the Ryukyus.

Mosquito membrane feeding assay. Heparinized syringes were used for peripheral blood collection, with written informed consent, from *P. vivax* patients who came to a malaria clinic in the Mae Sod district in the Tak province of northwestern Thailand. Single species infection with *P. vivax* was confirmed by Giemsa stain of thick and thin blood smears. The levels of parasitemias and the gametocytemias were 0.22 and 0.02%, respectively, for the volunteer *P. vivax* patient 1, and 0.23 and 0.01%, respectively, for the volunteer *P. vivax* patient 2. Collected blood was aliquoted into tubes (300 μl/tube), and the plasma was removed after brief centrifugation. Pooled mouse antisera were mixed with an equal volume of heat-inactivated normal human AB serum prepared from malaria-naive donors. The test antiserum sample was mixed and incubated with *P. vivax*-infected blood cells (1:1 [vol/vol] ratio) for 15 min at room temperature. The mixture was then applied to a membrane feeding apparatus kept at 37°C to allow starved *Anopheles dirus* A mosquitoes (Bangkok colony, Armed Forces Research Institute of Medical Sciences) to feed on the blood meals for 30 min. Fully engorged mosquitoes were separated from unfed mosquitoes, maintained for a week in an insectary kept at 26°C, and provided with 10% sucrose water. For each blood sample-serum mixture, 20 mosquitoes were dissected, and the number of oocysts in the midgut was counted under a microscope after 0.5% mercurochrome staining.

All human subject research conducted in the present study was reviewed and approved by the Ethics Committee of the Thai Ministry of Public Health and the Institutional Review Board of the Walter Reed Army Institute of Research.

Detection of native Pvs25 in antisera from immunized mice. Peripheral blood from *P. vivax*-infected patients was collected as described above. The gametocytemic patient blood was used to grow zygotes and ookinetes *in vitro*, as described previously (23). They were spotted onto slides and fixed with acetone as described previously (1–3). The slides were blocked with 5% nonfat milk in PBS and incubated with mouse antisera derived from immunization with CTB-Pvs25H-A fusion protein emulsified with IFA or with the fusion protein supplemented with CT (1 μg), after dilution of the antisera 100-fold with 5% nonfat milk in PBS. The samples were washed with ice-cold PBS and incubated with Alexa 488-conjugated anti-mouse antibody (Invitrogen, Carlsbad, CA). After a wash with ice-cold PBS, the slides were viewed by confocal scanning laser microscopy (LSM5 Pascal; Carl Zeiss MicroImaging, Thornwood, NY).

Statistical analysis. The Wilcoxon-Mann-Whitney test was used to compare antibody titers or the number of oocysts per mosquito between the nonimmune and an indicated immunization group or between indicated two immunization groups. The Kruskal-Wallis test was used to compare antibody titers or the number of oocysts per mosquito among three groups (i.e., S, M, and L). The chi-square test was used to analyze the difference in the proportion of parasite-free mosquitoes out of the total number of mosquitoes examined between the nonimmune and an indicated immunization group or between indicated two immunization groups. All statistical analysis were conducted by using JMP software version 8.0 (SAS Institute, Inc., Cary, NC).

RESULTS

Expression and purification of recombinant Pvs25H-A isoform from *P. pastoris*. Ookinete surface proteins (OSPs) contain several intramolecular disulfide bonds, e.g., the 11 disulfide bonds in Pvs25, which are important for overall structural integrity and native antigenicity. For this reason, *E. coli* expression systems are unsuitable, and therefore yeast *Saccharomyces cerevisiae* expression systems are used (12, 15, 19, 22). We explored other, more efficient recombinant protein expression systems for Pvs25 and found a higher production efficiency in the yeast *P. pastoris*. We constructed a plasmid for secretory expression of Pvs25 as a C-terminal hexahistidine-tagged protein (Pvs25H) (Fig. 1a). The culture supernatant of recombinant *P. pastoris* was found to contain several protein species that were not present in the culture supernatant of vector-transformed clones (Fig. 1b), and these protein bands specifically reacted with anti-Pvs25 antiserum, as well as with an anti-hexahistidine tag monoclonal antibody (data not shown). Secreted Pvs25H was affinity purified on a nickel Sepharose column and further separated into large (fractions 16 to 19) and small (fractions 21 to 23) protein species by size exclusion chromatography (Fig. 1c and d). At least five protein bands were identified on SDS-PAGE (Fig. 1b) and their corresponding peaks by size exclusion chromatography (fractions 16, 17, 18-19, 21-22, and 22-23 in Fig. 1c and d). The apparent molecular masses of these protein species based on gel mobility on SDS-PAGE were estimated to be 63.2, 47.3, 33.2, 16.1, and 28.3 kDa, respectively. The calculated molecular mass of Pvs25H (based on its deduced amino acid sequence) is 20.2 kDa, to which the fraction 21 and 22 protein species corresponded most closely. We therefore concluded that this was monomeric Pvs25H. Furthermore, the apparent molecular masses of protein species found in fractions 18 and 19, 17, and 16 corresponded very well to multiples of the molecular mass of the apparent monomer, so we concluded that they represented the dimer, trimer and tetramer of Pvs25H, respectively. The protein species that appeared in fractions 22 and 23 exhibited markedly different gel mobility (28.3 kDa) from that of the monomeric protein (16.1 kDa) (Fig. 1d), although these two showed extensively overlapping chromatographic peaks on size exclusion chromatography (Fig. 1c). We concluded that the protein species in fractions 22 and 23 was a monomeric protein with a distinct hydrophobic character, and thus decided to further separate these two monomers based on hydrophobicity profile by HIC. HIC clearly separated the two monomeric isoforms (Fig. 1f), and we named the less hydrophobic isoform and the more hydrophobic isoform the A and B monomeric isoforms, respectively (19). The observed lower gel mobility for the A isoform than the B isoform on SDS-PAGE under nonreducing conditions (Fig. 1d) was consistent with the results of HIC: the more hydrophilic the molecule, the fewer SDS molecules bind, and the protein becomes less negatively charged, resulting in reduced gel mobility on SDS-PAGE.

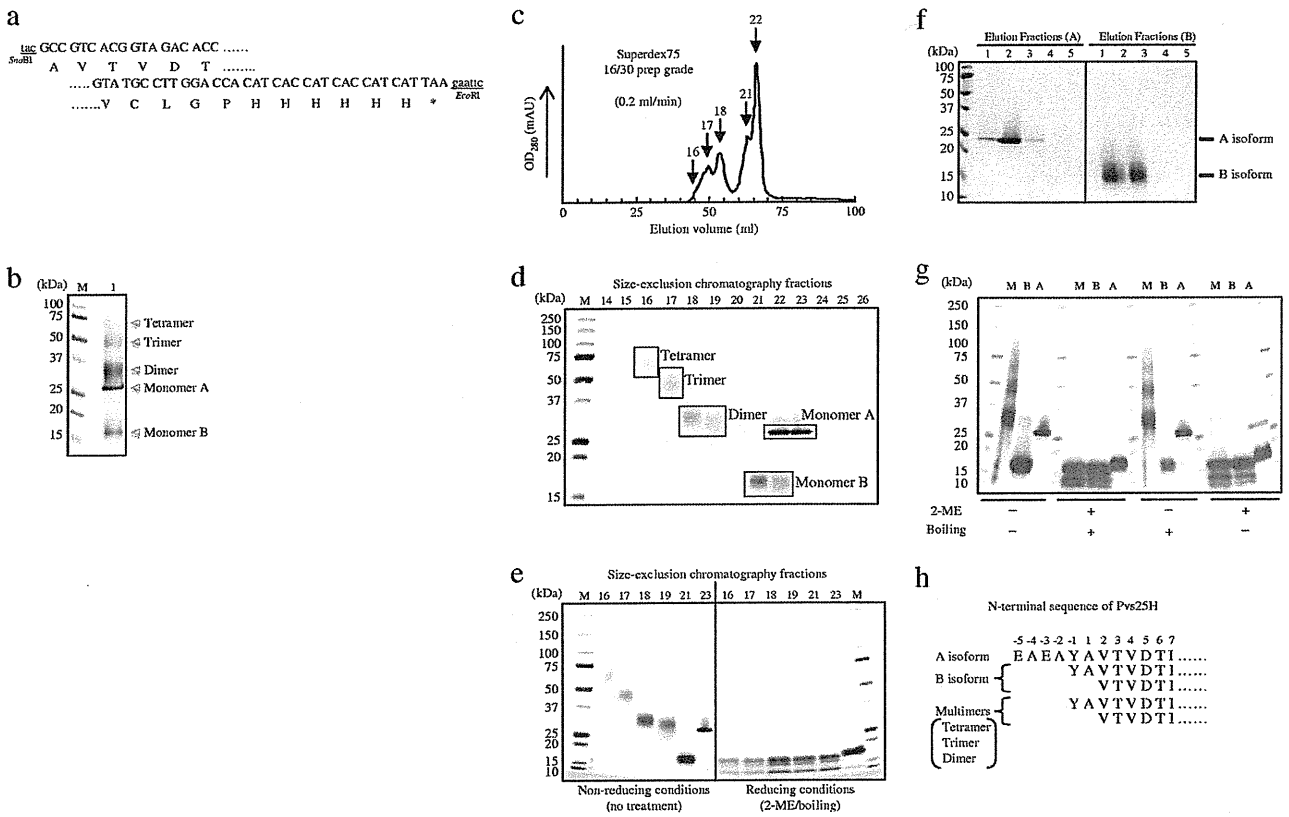

FIG. 1. Construction and expression analysis of Pvs25H in *Pichia pastoris*. (a) The 5′- and 3′-coding regions of the *Pvs25* gene sequence with its predicted amino acid sequence (Ala_{23} to Leu_{195}). The *Pvs25* gene fused to a hexahistidine tag at its C terminus was inserted into the SnaBI and EcoRI sites of pPIC9K, and the gene was integrated into the chromosomal DNA of *P. pastoris* strain GS115 by homologous recombination. (b) After selection of a high-producer clone that secreted the recombinant protein, nickel-affinity chromatography-purified Pvs25H was analyzed by SDS-PAGE (lane 1). M, molecular marker. (c) The affinity-purified Pvs25H was fractionated by size exclusion chromatography from which at least five chromatographic peaks were observed. (d) Size exclusion chromatography fractions 14–26 were subjected to SDS-PAGE (15% acrylamide). Based on the apparent molecular mass of each protein band, the fractions 16, 17, 18-19, 21-22, and 22-23 were defined as the tetramer, trimer, dimer, monomer B, and monomer A, respectively. (e) Selected chromatography peaks were subjected to 5 to 20% acrylamide gradient SDS-PAGE under nonreducing or reducing (10% 2-ME and boiling) conditions. (f) Hydrophobic interaction chromatography of the Pvs25H-A and Pvs25H-B monomeric isoforms. Elution fractions (A) are eluates of 2 M NH_4SO_4 (Pvs25H-A) and elution fractions (B) are eluates of PBS (Pvs25H-B). (g) Each isoform (M, a mixture of dimer, trimer and tetramer; B, B isoform; A, A isoform) was subjected to 15% acrylamide SDS-PAGE under various conditions, as indicated. (h) The N-terminal protein sequence of each isoform. Positively numbered amino acid residues (Ala_1 and the following) are residues of the Pvs25 protein; negatively numbered amino acids are derivatives of the pPIC9K α-factor secretion signal. The A monomer revealed a single, unique sequence, but the B monomer and the multimers showed a mixture of different N termini.

Molecular characterization of Pvs25H isoforms. The A isoform appeared as a single sharp band, but the other isoforms, including the multimers and the B monomer, appeared as diffuse bands on SDS-PAGE (Fig. 1b and d to g), indicating that the A isoform is constrained to a more uniform molecular configuration than the other isoforms. In addition, all of the isoforms, except the A isoform, generated at least three identical protein bands when samples were heat treated in the presence of SDS and β-mercaptoethanol (2-ME) prior to SDS-PAGE. The A isoform appeared as a single protein band with a slightly higher molecular mass than that for the largest protein band among the three bands observed for the other isoforms (Fig. 1e).

To characterize the molecular configuration of each isoform furthermore, mixtures of the multimers, including dimers, trimers, and tetramers and the A and B monomers, were subjected to SDS-PAGE after various treatments, as indicated in Fig. 1g. The gel mobility of all of the isoforms did not show any noticeable changes after boiling (100°C, 2 min), but 2-ME treatment (10% [vol/vol]) resulted in a banding pattern very similar to the pattern observed for complete denaturation (2-ME and boiling), except that the A isoform seemed to be slightly more resistant to the reducing agent than the other isoforms. This became particularly notable when lower concentrations of the reducing agent were used (data not shown). These results suggest that the multimers comprised B monomers self-cross-linked by intermolecular disulfide bonds and that the A isoform has a higher molecular rigidity than the other isoforms. Because all of the isoforms exhibited a strong resistance to the boiling and SDS, but not to the 2-ME and SDS treatment, it is plausible that the physical integrity of the protein is critically, if not completely, maintained by disulfide bonds.

Next, to evaluate the status of the covalent disulfide bonds in

the Pvs25H protein, Ellman's test was conducted for each isoform. No isoform reacted with the Ellman's reagent, suggesting either that no reduced sulfhydryls were present or that the molecules were inaccessible to the reagent. However, treatment with TCEP immobilized on agarose prior to the Ellman's test resulted in the detection of 4 to 6 molecules of reduced sulfhydryls per molecule of B monomer or multimeric isoforms, but fewer than 0.3 molecules of reduced sulfhydryls were detected per molecule of A monomer. These results indicated that the B and multimeric isoforms have disulfide bonds that are more accessible to surface-immobilized TCEP than those of the A isoform, indicating that the A isoform has more deeply buried disulfide bonds than the other isoforms. It is indicative of the higher molecular flexibility of the B isoform and the multimers than of the A isoform. Interestingly, however, denaturation of proteins with 2% SDS or 6 M guanidine hydrochloride, or TCEP agarose treatment in the presence of these denaturants prior to the Ellman's test, did not further increase the level of free sulfhydryls. These results strongly support the notion that all of the isoforms are tightly packed molecules and that their rigidity is maintained by intramolecular disulfide bonds and other noncovalent interactions.

Finally, the N-terminal protein sequences determined by the Edman degradation method for each isoform supported the results of SDS-PAGE, in that the multimers and the B isoform contain a mixture of polypeptide species with multiple N termini; however, the A isoform comprises a single polypeptide with a longer, unique N terminus (Fig. 1h). These results suggested that the multimers and the B isoform contain the same set of polypeptide species, with multiple primary structures and presumably various folding configurations. By using different combinations of structurally heterologous polypeptides, different isoforms might be generated.

Taken together, we concluded that the A isoform, which has a more uniform protein configuration, is less hydrophobic and has higher molecular rigidity than the B isoform, and perhaps it most closely resembles the native Pvs25 protein at the structural level. The proportions of each isoform expression were estimated to be 42% (A isoform), 27% (B isoform), 16% (dimer), 10% (trimer), and 5% (tetramer). Thus, the A isoform was produced most abundantly among all of the isoforms. The final protein yields of the total Pvs25H and the A isoform using our expression and purification method were 30 to 50 mg and 12 to 20 mg/liter of culture medium, respectively. We confirmed that the purified Pvs25H-A contained endotoxin at levels less than 0.05 EU/μg of protein. Based on these observations, we decided to use the A isoform (Pvs25H-A) as a TBV antigen to be linked to CTB.

Chemical conjugation of Pvs25H-A to CTB and its molecular evaluation. Recombinant CTB was expressed by *P. pastoris* strain GS115 and purified as previously reported (11). Pvs25H-A was chemically conjugated to CTB by using the heterobifunctional cross-linker SPDP (Fig. 2). Because CTB contains two cysteine residues per monomeric subunit, which, in the native form, are involved in an intramolecular disulfide bond, the existence of reduced sulfhydryls in our recombinant CTB was determined by using Ellman's reagent, and none was detected (data not shown).

Various conjugation schemes were evaluated for efficiency of linking Pvs25H-A to CTB via SPDP (Fig. 2a and b). Consistent with the results of Ellman's test for Pvs25H-A and CTB, SPDP modification of only one protein failed to generate the CTB-Pvs25H-A fusion complex (Fig. 2b). Thus, at least one partner protein had to be treated with the reducing agent to expose free sulfhydryls and make it reactive toward the pyridyldithiol groups added to the partner protein. Because intact disulfide bonds might be important for the overall structural integrity and native antigenicity of Pvs25 (12, 15, 19, 22), we avoided treating it with reducing agents. Therefore, the CTB or SPDP-modified CTB (CTB^{SPDP}) was treated instead with DTT (designated as CTB^{DTT} or $CTB^{SPDP/DTT}$ in Fig. 2a). Although both CTB^{DTT} and $CTB^{SPDP/DTT}$, when reacted with SPDP-modified Pvs25H-A (Pvs25H-A^{SPDP}), generated substantial levels of fusion complex with retained affinity for GM1-ganglioside, sequential treatment of CTB with SPDP and then with DTT resulted in an even higher specific reactivity toward Pvs25 antiserum (Fig. 2b).

Second, to evaluate the homogeneity of the fusion complex and the stoichiometry of each component within the complex, proteins before and after the conjugation process were analyzed by size exclusion chromatography (Fig. 2c). The two chromatographic peaks for Pvs25H-A and CTB in a mixed sample disappeared, and a new single peak emerged with an apparent molecular mass of 97.2 kDa. Because the molecular masses of Pvs25H-A and CTB are 29.8 and 53.4 kDa, respectively, based on the K_{av} values of chromatography standard proteins, the average stoichiometric ratio for CTB and Pvs25H-A was calculated to be 1:1.5, indicating that one CTB pentamer molecule carries one to two molecules of Pvs25H-A on its surface. Alternatively, if it is assumed that the fusion complex is highly homogeneous and its stoichiometric ratio is 1:1, the 14-kDa discrepancy between the observed and calculated fusion complex mass may be explained by irregularities in the molecular shape, resulting in a higher apparent molecular mass.

Taking all of the results together, we decided to use the Pvs25H-A^{SPDP} + $CTB^{SPDP/DTT}$ conjugation method (Fig. 2d) to generate the fusion complex for all immunization experiments.

Immunogenicity in mice of Pvs25H-A and its fusion protein with CTB when administered by the s.c. or the i.n. route. BALB/c mice were immunized with Pvs25H-A (designated as "S" in Fig. 3 and 4), a mixture of Pvs25H-A and CTB (designated as "M" in Fig. 3 and 4), or CTB-Pvs25H-A fusion protein (designated as "L" in Fig. 3 and 4), by the s.c. or the i.n. route, with or without the indicated adjuvants, at weeks 0, 2, and 3. Antisera were collected at week 4, and the Pvs25H-A-specific IgG titers were determined (Fig. 3a). We demonstrated that: (i) s.c. immunization tended to induce a higher response than i.n. immunization in both the absence and the presence of adjuvants; (ii) the fusion protein (L) consistently induced a higher response than antigen alone (S) or the mixture of proteins (M), regardless of adjuvant supplementation; (iii) supplementation with adjuvants was required for substantial augmentation of the IgG response for both immunization routes; (iv) IFA significantly augmented the response elicited by unfused or CTB-mixed antigen, but CT only marginally affected the response elicited by these antigens; and (v) CT did not exhibit a dose-dependent augmentation effect on the IgG response in the dose range used in the present study (0.1 to 1.0

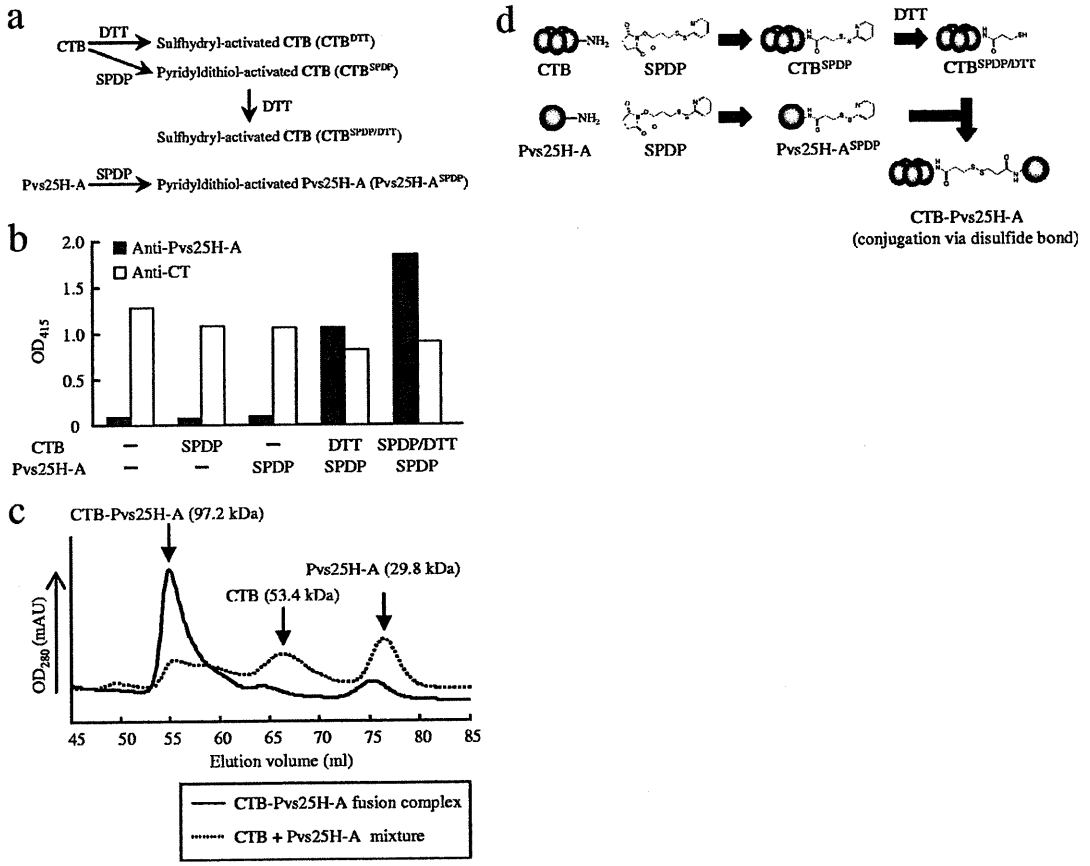

FIG. 2. Chemical conjugation of Pvs25H-A to cholera toxin B subunit (CTB). Various conjugation methods were evaluated for the generation of the CTB-Pvs25H-A fusion complex. The heterobifunctional cross-linker *N*-succinimidyl 3-(2-pyridyldithio) propionate (SPDP) was used to link Pvs25H-A to CTB via the primary amines. (a) Either CTB or SPDP-modified CTB (CTB^{SPDP}) was first treated with DTT to expose free sulfhydryls (designated as CTB^{DTT} and $CTB^{SPDP/DTT}$, respectively), and then SPDP-modified Pvs25H-A ($Pvs25H\text{-}A^{SPDP}$) was separately mixed with each of them to generate the fusion complex. (b) The CTB-Pvs25H-A fusion complex was analyzed by GM1-ELISA using anti-cholera toxin (CT) (□) or anti-Pvs25H-A (■) antiserum. (c) The CTB-Pvs25H-A fusion protein (solid line) or a mixture of CTB and Pvs25H-A (dotted line) was subjected to size exclusion chromatography. For the fusion protein, the peaks for CTB and Pvs25H-A disappeared, and a new peak emerged, indicating generation of the fusion complex. (d) The conjugation scheme chosen for production of the CTB-Pvs25H-A fusion complex. See Materials and Methods for the detailed conjugation method.

μg). Finally, we confirmed that the antisera specifically recognized the *P. vivax* ookinete surface by immunofluorescence (Fig. 3b).

Transmission-blocking effect of the induced mouse antisera against field strains of *P. vivax* parasites. The TBV efficacy of the induced mouse antisera against *P. vivax* parasites in infected blood samples from patients was evaluated by the membrane feeding assay. The same experiments were performed twice, using blood samples from two volunteer donors (Fig. 4). The average number of oocysts observed per mosquito fed on patient blood mixed with antisera induced by s.c. immunization of mice with Pvs25H-A/IFA was reduced by >99.9% compared to the naive control serum (N). Omission of the adjuvant significantly abated the effect down to 20 to 60% reduction; however, conjugating the antigen to CTB resulted in a dramatic restoration of the vaccine efficacy back to >90%. A similar tendency, albeit with significantly lower efficacy, was observed for i.n. immunization, in that antisera induced by i.n. immunization with the fusion protein decreased the oocyst number by 70 to 90%, whereas unfused antigen conferred only a 0 to 6% blocking effect. As expected, CT supplementation augmented the effect for i.n.-administered antigens, in that both unfused and CTB-fused antigens conferred a blocking effect of >90%. Interestingly, however, addition of CTB to the mixture of antigen and CT significantly abated the vaccine efficacy down to 40 to 50%. The reason for this is unknown, and it could not have been predicted from the antibody titers (Fig. 3a). Taken together, we concluded that chemical coupling of Pvs25 to CTB is a potentially promising strategy to enhance the transmission-blocking efficacy in i.n. and s.c immunization regimes.

DISCUSSION

Pvs25 is one of the top-priority *P. vivax* TBV candidates, and the production of stable and functional forms of the antigen in the most appropriate formulation is crucial (4; MVTR). In the present study, we investigated the methylotrophic yeast *P. pas-*

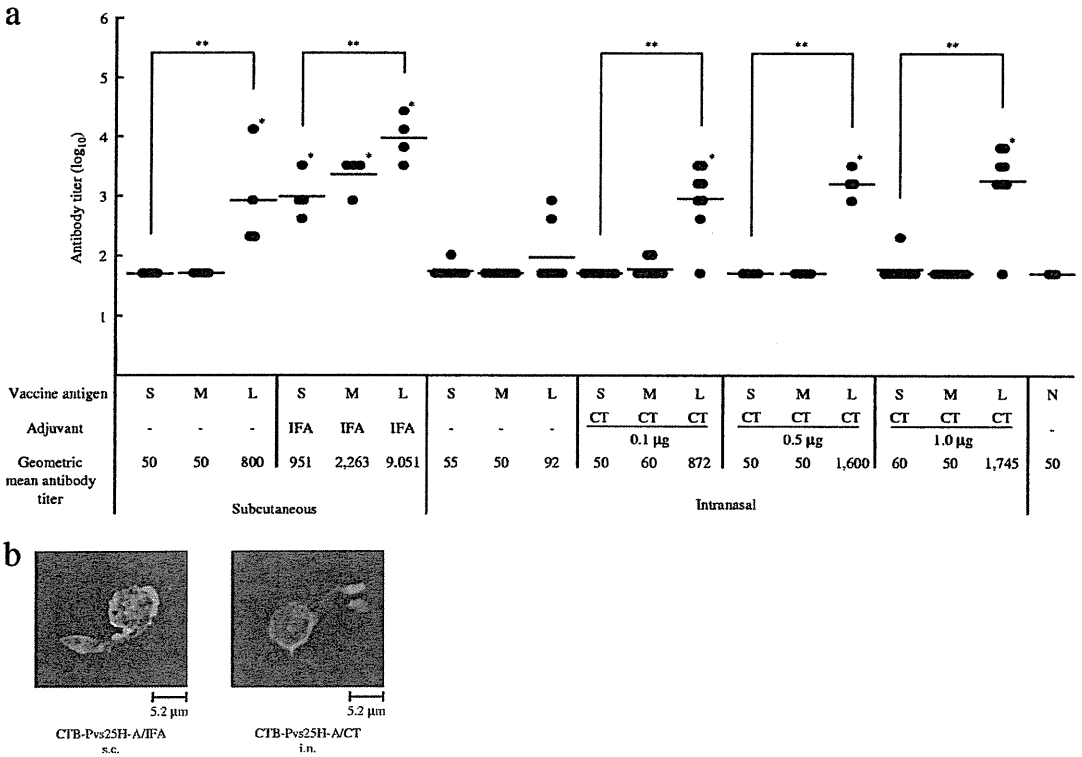

FIG. 3. Immunogenicity of the CTB-Pvs25H-A fusion protein for induction of a Pvs25-specific serum IgG response. (a) Female BALB/c mice (four or eight mice per group) were immunized with Pvs25H-A alone (30 μg) (S), a mixture of cholera toxin B subunit (CTB; 30 μg) and Pvs25H-A (30 μg) (M), or the CTB-Pvs25H-A fusion protein (60 μg), by the subcutaneous (s.c.) or the intranasal (i.n.) route (L), three times, at weeks 0, 2, and 3. Serum samples were collected a week after the third immunization and were evaluated for Pvs25-specific IgG titers. All mice received the same amount of Pvs25H-A antigen, i.e., 30 μg per injection. IFA and CT at various doses (0.1 to 1.0 μg) were used as s.c. and i.n. vaccine adjuvants, respectively. Nonimmune serum (N) was used as a negative control. Antibody titers were defined as the serum dilution that gave an OD_{415} of 0.1 or the serum dilution for which a one-point-higher dilution (2-fold) gave an OD_{415} of <0.1. *, Significantly different from nonimmune serum as determined by the Wilcoxon-Mann-Whitney test ($P < 0.05$); **, significantly different among the three groups (S, M, and L) as determined by the Kruskal-Wallis test ($P < 0.001$). (b) Ookinete-specific reactivity of induced antisera analyzed by immunofluorescence. The antisera derived from s.c. immunization with the CTB-Pvs25H-A fusion protein emulsified with IFA (CTB-Pvs25H-A/IFA), or the fusion protein administered i.n. with CT (1 μg) (CTB-Pvs25H-A/CT) specifically recognized native Pvs25 protein expressed on the surface of *Plasmodium vivax* ookinetes. Scale bar, 5.2 μm.

toris as a production host for Pvs25. The yield of Pvs25H was comparable to that reported previously for its expression in *S. cerevisiae* (19). When expressed in *S. cerevisiae*, this protein was also produced as a mixture of various isoforms (19). Although we observed a similar protein expression pattern, i.e., multimers and the A and B monomers, higher proportions of the molecularly homogeneous A isoform than the heterogeneous B and multimeric isoforms were produced when Pvs25H was expressed in *P. pastoris* and not in *S. cerevisiae*. This might present an advantage of using *P. pastoris* expression system for Pvs25 vaccine production rather than *S. cerevisiae* system. The *P. pastoris*-derived A isoform could be as conveniently and efficiently purified from the culture supernatant as reported for *S. cerevisiae*-derived A isoform, by a combination of affinity, size exclusion, and hydrophobic interaction chromatographies.

The next critical step in vaccine generation is the optimization of vaccine antigen formulations; a search for the optimal antigen formulation is often considered to be as important as choosing the best antigen among many vaccine candidate antigens. Pvs25H antigen adsorbed onto Alhydrogel (Brentag Biosector, Frederilssund, Denmark) has recently been shown to induce antibody effectively in human volunteers in a phase 1 clinical trial, and the antigen was found to be efficacious, as evidenced by significant transmission-blocking activity observed in the membrane feeding assay (17). That study confirmed that Pvs25 is a very promising TBV candidate; however, it is highly desirable to induce higher levels of transmission-blocking immunity for practical vaccine development (17). Another phase 1 clinical trial using Montanide ISA 51, a water-in-oil emulsion, has recently been completed; however, due to an unexpected frequent local reactogenicity, the vaccine efficacy has not been verified (29). Therefore, there seems to be an increasing demand for the development of a new immune-enhancing vaccine platform technology for malaria OSPs, because they are low-molecular-weight proteins that are by themselves not sufficiently immunogenic.

There have been several reports showing examples of chemical conjugation of *Plasmodium falciparum* OSPs with potential antigen carrier molecules such as the outer membrane protein of *Neisseria meningitidis* (30), exoprotein A of *Pseudomonas*

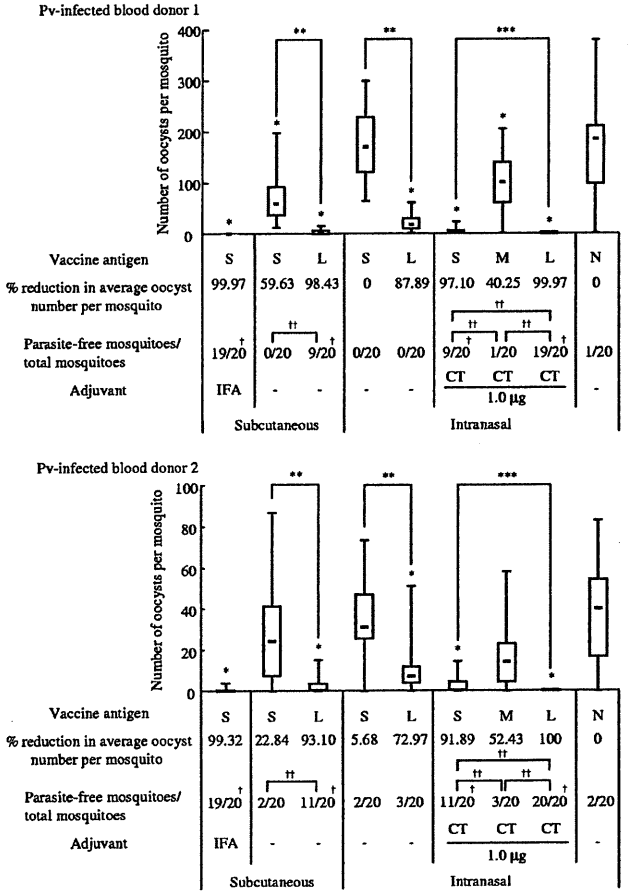

FIG. 4. Transmission-blocking vaccine (TBV) effects of the induced mouse antisera on *Plasmodium vivax* oocyst development in the *Anopheles dirus* A mosquito midgut. TBV effects on oocyst numbers induced by antisera (1/2 dilution) obtained from mice immunized with each antigen formulation (S, M, and L) as described in Fig. 3. N, nonimmune serum. Either IFA or CT was used as an adjuvant, as indicated. The data are expressed as the median values of oocyst number found per mosquito (bar within the box) with the 25 and 75% quartiles (the box) and ranges (whiskers above and below the box). The percent reduction was calculated as the reduction in the average oocyst number for each immunization group compared to the average oocyst number for the unimmunized control group (N). The number of parasite-free mosquitoes per total number of mosquitoes examined (20 mosquitoes) is provided. The analysis was performed twice, using different blood samples, as indicated in the upper panel (*P. vivax* [Pv]-infected blood donor 1) and the lower panel (Pv-infected blood donor 2). M groups without adjuvant supplementation, M and L groups with IFA supplementation, and all groups with 0.1- and 0.5-μg CT supplementation were excluded from membrane feeding analysis. *, $P < 0.001$ versus the nonimmune (N) group as determined by the Wilcoxon-Mann-Whitney test; **, $P < 0.001$ between the S and L groups as determined by the Wilcoxon-Mann-Whitney test; ***, $P < 0.001$ among the three groups (S, M, and L) as determined by the Kruskal-Wallis test; †, $P < 0.005$ versus the nonimmune (N) group as determined by the chi-square test; ††, $P < 0.005$ between the indicated two groups as determined by the chi-square test.

aeruginosa (16), ovalbumin (16), and a *P. falciparum* OSP itself by chemical crosslinking (16). All of these were demonstrated to increase TBV efficacy, but no attempts have yet been made to enhance the immunogenicity of *P. vivax* OSPs by coupling them to other proteins. In the present study we evaluated CTB as a potential carrier for Pvs25. First, to extend our previous study where CT was used as adjuvant (1–3), we tested our hypothesis that the mucosal immunogenicity of Pvs25 would increase when the protein was coupled to the nontoxic CTB subunit, even in the absence of CT supplementation. Second, to explore CTB's less-characterized immune potentiating properties for s.c.-delivered antigens, we immunized mice with the CTB-Pvs25H-A fusion protein by an s.c. route, in the presence or absence of IFA. Our principal finding was that the coupling of the antigen to CTB profoundly enhanced its immunogenicity in i.n. as well as in s.c. immunization regimes, without supplementation with extraneous adjuvants. However, the membrane feeding assay revealed that there was still much room for improvement (Fig. 4). For instance, although i.n. administration of the fusion protein alone conferred a relatively high transmission-blocking immunity (88 and 73% decreases in oocyst number for blood samples from donors 1 and 2, respectively) compared to unfused antigen alone or the unimmunized control group, only a few mosquitoes (0/20 to 3/20) were free of parasites. Supplementation of CT to the fusion protein increased the efficacy close to complete blockade (>99.9%), significantly increasing the number of mosquitoes free of parasites (19/20 to 20/20). Because supplementation of CT to unfused antigen resulted in an intermediate level of protection (97% [9/20] and 92% [11/20] decrease in oocyst number for blood samples from donors 1 and 2, respectively), we concluded that both the CT supplementation and the CTB-coupling strategies contributed to the increased vaccine efficacy, although the former was more efficient than the latter. A similar tendency was observed for the s.c. immunization regime: s.c. administration of the fusion protein alone conferred a more than 90% decrease in oocyst number, in which approximately half of the mosquitoes were free of parasites (9/20 to 11/20); however, the use of IFA with unfused antigen contributed more than the fusion method. We observed that the efficacy of the fusion protein administered alone by the s.c. route was almost equal to that attained by the unfused antigen administered i.n. with CT supplementation, in terms of the average numbers of oocyst per mosquito (>90%) as well as the number of mosquitoes free of parasites (9/20 to 11/20). Similarly, the vaccine efficacy for unfused antigen administered s.c. with IFA was almost equal to the level attained by the fusion protein administered i.n. with CT in terms of the average number of oocysts per mosquito (>99%) as well as the number of mosquitoes free of parasites (19/20 to 20/20). Although we did not assess the vaccine efficacy of the fusion protein emulsified in an oil adjuvant such as IFA, IFA was very effective in that almost complete blockade was observed for unfused antigen. It is likely that a combination of oil adjuvant and the CTB-coupling strategy would further enhance the efficacy. Taken together, we conclude that (i) s.c. immunization is more efficacious than i.n. immunization, inducing "one-level-higher" immunity than i.n. immunization, and (ii) a CTB-coupling strategy is substantially effective in enhancing transmission-blocking immunity, but supplementation with extraneous adjuvants is expected to induce an even higher immunity (Fig. 5).

The clinical use of CT, particularly as a nasal adjuvant, is hampered by its toxicity (26). Furthermore, the nontoxic CTB has yet to be proven a safe nasal vaccine delivery molecule.

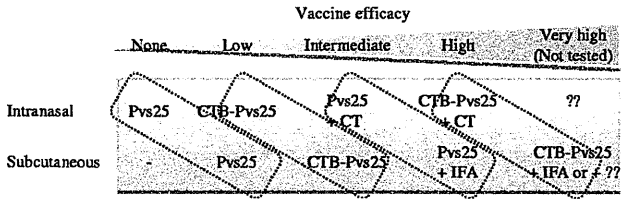

FIG. 5. Schematic summary of the observed or expected (but not tested) transmission-blocking vaccine (TBV) efficacy induced by each immunization regime. s.c. immunization tended to induce "one-level-higher" immunity than i.n. immunization in our experimental model. Identical or similar vaccine formulations are encircled by a dotted line. CTB, cholera toxin B subunit; CT, cholera toxin; IFA, incomplete Freund's adjuvant.

Therefore, an alternative approach for using CTB as a vaccine antigen carrier is highly desirable. Although there have been numerous reports demonstrating enhanced mucosal immunogenicity of various antigens by coupling to CTB (13), very few systematic studies have been conducted to assess CTB's antigen carrier capacity for s.c.-delivered antigens. Our present study clearly demonstrated the potential of CTB in s.c. vaccine platform design. Furthermore, it is notable that, unlike antigens emulsified with oil adjuvant such as IFA or antigens administered with an aluminum hydroxide adjuvant, the protein-only CTB-coupled antigens are likely to be much less reactogenic. It is believed that recent innovations in effective but much less locally reactogenic and safer oil adjuvants such as MF59 (Chiron Corp., Emeryville, CA) (20, 21), the Montanide ISA series (Seppic, Inc., Fairfield, NJ) (20, 29), and the GlaxoSmithKline adjuvant systems (GlaxoSmithKline, Brentford, United Kingdom) (8, 27), will expedite malaria vaccine development. It is also possible that protein delivery molecules will ultimately be combined with effective oil or other adjuvants, including aluminum hydroxide. This is supported by our recent unpublished study in which a recombinant malaria antigen administered with an alum adjuvant only marginally enhanced its immunogenicity, whereas the same antigen loaded onto carrier molecules became highly immunogenic when applied together with the alum.

In the present study, we did not assess the molecular mechanisms of the immune potentiating function of CTB. However, our observation that simple mixing of Pvs25H-A with CTB did not produce a profound immune enhancement implies that its immunogenicity results from the antigen delivery, rather than a physiological cell activation, as occurs for CT. Further experiments are ongoing to characterize the immune potentiating function of CTB using the C-terminal 19-kDa fragment of merozoite surface protein 1 from *Plasmodium yoelii*. The results of these studies will help us judge whether CTB could contribute to a new platform technology for the design of s.c.-delivered subunit vaccines against infectious diseases such as malaria.

ACKNOWLEDGMENTS

We thank the staff of the Department of Entomology, Armed Forces Research Institute of Medical Sciences, Bangkok, Thailand, for their technical assistance.

This study was supported by the following grants: the Program of Founding Research Centers for Emerging and Reemerging Infectious Diseases from the Ministry of Education, Culture, Sports, Science and Technology, Japan (MEXT); Grants-in-Aid for Scientific Research (19406009 and 20590425) and Scientific Research on Priority Areas (21022034) from MEXT; a grant from The Okinawa Industry Promotion Public Corp. (Naha, Okinawa, Japan); and a Cooperative Research Grant from NEKKEN, 2010.

REFERENCES

1. **Arakawa, T., A. Komesu, H. Otsuki, J. Sattabongkot, R. Udomsangpetch, Y. Matsumoto, N. Tsuji, Y. Wu, M. Torii, and T. Tsuboi.** 2005. Nasal immunization with a malaria transmission-blocking vaccine candidate, Pfs25, induces complete protective immunity in mice against field isolates of *Plasmodium falciparum*. Infect. Immun. **73:**7375–7380.
2. **Arakawa, T., M. Tachibana, T. Miyata, T. Harakuni, H. Kohama, Y. Matsumoto, N. Tsuji, H. Hisaeda, A. Stowers, M. Torii, and T. Tsuboi.** 2009. Malaria ookinete surface protein-based vaccination via the intranasal route completely blocks parasite transmission in both passive and active vaccination regimens in a rodent model of malaria infection. Infect. Immun. **77:**5496–5500.
3. **Arakawa, T., T. Tsuboi, A. Kishimoto, J. Sattabongkot, N. Suwanabun, T. Rungruang, Y. Matsumoto, N. Tsuji, H. Hisaeda, A. Stowers, I. Shimabukuro, Y. Sato, and M. Torii.** 2003. Serum antibodies induced by intranasal immunization of mice with *Plasmodium vivax* Pvs25 co-administered with cholera toxin completely block parasite transmission to mosquitoes. Vaccine **21:**3143–3148.
4. **Arevalo-Herrera, M., C. Chitnis, and S. Herrera.** 2010. Current status of *Plasmodium vivax* vaccine. Hum. Vaccin. **6:**124–132.
5. **Bill and Melinda Gates Foundation.** 2009. Global health program. Bill and Melinda Gates Foundation, Seattle, WA. http://www.gatesfoundation.org/global-health/Documents/malaria-strategy.pdf.
6. **Birkett, A. J.** 2010. PATH Malaria Vaccine Initiative (MVI): perspectives on the status of malaria vaccine development. Hum. Vaccin. **6:**139–145.
7. **Carter, R.** 2001. Transmission blocking malaria vaccines. Vaccine **19:**2309–2314.
8. **Garcon, N., P. Chomez, and M. Van Mechelen.** 2007. GlaxoSmithKline adjuvant systems in vaccines: concepts, achievements and perspectives. Expert Rev. Vaccines **6:**723–739.
9. **Genton, B.** 2008. Malaria vaccines: a toy for travelers or a tool for eradication? Expert Rev. Vaccines **7:**597–611.
10. **Greenwood, B. M., D. A. Fidock, D. E. Kyle, S. H. Kappe, P. L. Alonso, F. H. Collins, and P. E. Duffy.** 2008. Malaria: progress, perils, and prospects for eradication. J. Clin. Invest. **118:**1266–1276.
11. **Harakuni, T., H. Sugawa, A. Komesu, M. Tadano, and T. Arakawa.** 2005. Heteropentameric cholera toxin B subunit chimeric molecules genetically fused to a vaccine antigen induce systemic and mucosal immune responses: a potential new strategy to target recombinant vaccine antigens to mucosal immune systems. Infect. Immun. **73:**5654–5665.
12. **Hisaeda, H., A. W. Stowers, T. Tsuboi, W. E. Collins, J. S. Sattabongkot, N. Suwanabun, M. Torii, and D. C. Kaslow.** 2000. Antibodies to malaria vaccine candidates Pvs25 and Pvs28 completely block the ability of *Plasmodium vivax* to infect mosquitoes. Infect. Immun. **68:**6618–6623.
13. **Holmgren, J., J. Adamsson, F. Anjuere, J. Clemens, C. Czerkinsky, K. Eriksson, C. F. Flach, A. George-Chandy, A. M. Harandi, M. Lebens, T. Lehner, M. Lindblad, E. Nygren, S. Raghavan, J. Sanchez, M. Stanford, J. B. Sun, A. M. Svennerholm, and S. Tengvall.** 2005. Mucosal adjuvants and anti-infection and anti-immunopathology vaccines based on cholera toxin, cholera toxin B subunit and CpG DNA. Immunol. Lett. **97:**181–188.
14. **Kaslow, D. C.** 1997. Transmission-blocking vaccines: uses and current status of development. Int. J. Parasitol. **27:**183–189.
15. **Kaslow, D. C., I. C. Bathurst, T. Lensen, T. Ponnudurai, P. J. Barr, and D. B. Keister.** 1994. *Saccharomyces cerevisiae* recombinant Pfs25 adsorbed to alum elicits antibodies that block transmission of *Plasmodium falciparum*. Infect. Immun. **62:**5576–5580.
16. **Kubler-Kielb, J., F. Majadly, Y. Wu, D. L. Narum, C. Guo, L. H. Miller, J. Shiloach, J. B. Robbins, and R. Schneerson.** 2007. Long-lasting and transmission-blocking activity of antibodies to *Plasmodium falciparum* elicited in mice by protein conjugates of Pfs25. Proc. Natl. Acad. Sci. U. S. A. **104:**293–298.
17. **Malkin, E. M., A. P. Durbin, D. J. Diemert, J. Sattabongkot, Y. Wu, K. Miura, C. A. Long, L. Lambert, A. P. Miles, J. Wang, A. Stowers, L. H. Miller, and A. Saul.** 2005. Phase 1 vaccine trial of Pvs25H: a transmission blocking vaccine for *Plasmodium vivax* malaria. Vaccine **23:**3131–3138.
18. **Mendis, K., B. J. Sina, P. Marchesini, and R. Carter.** 2001. The neglected burden of *Plasmodium vivax* malaria. Am. J. Trop. Med. Hyg. **64:**97–106.
19. **Miles, A. P., Y. Zhang, A. Saul, and A. W. Stowers.** 2002. Large-scale purification and characterization of malaria vaccine candidate antigen Pvs25H for use in clinical trials. Protein Expr. Purif. **25:**87–96.
20. **Peek, L. J., C. R. Middaugh, and C. Berkland.** 2008. Nanotechnology in vaccine delivery. Adv. Drug Deliv. Rev. **60:**915–928.
21. **Sachdeva, S., A. Mohmmed, P. V. Dasaradhi, B. S. Crabb, A. Katyal, P. Malhotra, and V. S. Chauhan.** 2006. Immunogenicity and protective efficacy

of *Escherichia coli* expressed *Plasmodium falciparum* merozoite surface protein-1_{42} using human compatible adjuvants. Vaccine **24:**2007–2016.
22. **Saxena, A. K., K. Singh, H. P. Su, M. M. Klein, A. W. Stowers, A. J. Saul, C. A. Long, and D. N. Garboczi.** 2006. The essential mosquito-stage P25 and P28 proteins from *Plasmodium* form tile-like triangular prisms. Nat. Struct. Mol. Biol. **13:**90–91.
23. **Suwanabun, N., J. Sattabongkot, T. Tsuboi, M. Torii, N. Maneechai, N. Rachapaew, N. Yim-amnuaychok, V. Punkitchar, and R. E. Coleman.** 2001. Development of a method for the in vitro production of *Plasmodium vivax* ookinetes. J. Parasitol. **87:**928–930.
24. **Targett, G. A., and B. M. Greenwood.** 2008. Malaria vaccines and their potential role in the elimination of malaria. Malar. J. **7**(Suppl. 1)**:**S10.
25. **Tsuboi, T., M. Tachibana, O. Kaneko, and M. Torii.** 2003. Transmission-blocking vaccine of vivax malaria. Parasitol. Int. **52:**1–11.
26. **van Ginkel, F. W., R. J. Jackson, Y. Yuki, and J. R. McGhee.** 2000. Cutting edge: the mucosal adjuvant cholera toxin redirects vaccine proteins into olfactory tissues. J. Immunol. **165:**4778–4782.
27. **Waitumbi, J. N., S. B. Anyona, C. W. Hunja, C. M. Kifude, M. E. Polhemus, D. S. Walsh, C. F. Ockenhouse, D. G. Heppner, A. Leach, M. Lievens, W. R. Ballou, J. D. Cohen, and C. J. Sutherland.** 2009. Impact of RTS,S/AS02(A) and RTS,S/AS01(B) on genotypes of *P. falciparum* in adults participating in a malaria vaccine clinical trial. PLoS One **4:**e7849.
28. **World Health Organization.** 2005. World health report. World Health Organization, Geneva Switzerland.
29. **Wu, Y., R. D. Ellis, D. Shaffer, E. Fontes, E. M. Malkin, S. Mahanty, M. P. Fay, D. Narum, K. Rausch, A. P. Miles, J. Aebig, A. Orcutt, O. Muratova, G. Song, L. Lambert, D. Zhu, K. Miura, C. Long, A. Saul, L. H. Miller, and A. P. Durbin.** 2008. Phase 1 trial of malaria transmission blocking vaccine candidates Pfs25 and Pvs25 formulated with montanide ISA 51. PLoS One **3:**e2636.
30. **Wu, Y., C. Przysiecki, E. Flanagan, S. N. Bello-Irizarry, R. Ionescu, O. Muratova, G. Dobrescu, L. Lambert, D. Keister, Y. Rippeon, C. A. Long, L. Shi, M. Caulfield, A. Shaw, A. Saul, J. Shiver, and L. H. Miller.** 2006. Sustained high-titer antibody responses induced by conjugating a malarial vaccine candidate to outer-membrane protein complex. Proc. Natl. Acad. Sci. U. S. A. **103:**18243–18248.

Editor: J. H. Adams

Chapter 8

An Efficient Approach to the Production of Vaccines Against the Malaria Parasite

Takafumi Tsuboi, Satoru Takeo, Tatsuya Sawasaki, Motomi Torii, and Yaeta Endo

Abstract

In malaria vaccine research, one of the major obstacles has been the difficulty of expressing recombinant malarial proteins and it is mainly due to the lack of an efficient methodology for the synthesis of sufficient quantity of quality proteins. We demonstrate that the wheat germ cell-free protein synthesis system can be applied for the successful production of leading malaria vaccine candidate antigens and, thus, prove that it may be a key tool for malaria vaccine research.

Key words: Cell-free protein synthesis, Parasite, Malaria, Vaccine

1. Introduction

Malaria, a serious infectious disease that challenges the global health, causes millions of deaths annually, as well as illness in hundreds of millions of people. The most deadly form of the disease is caused by the inoculation of the malaria parasite, *Plasmodium falciparum*, by infected mosquito bites. The disease is re-emerging mainly due to the emergence of multidrug-resistant parasites and insecticide-resistant mosquitoes (1). Therefore development of malaria vaccine has been considered as one of the essential components for the malaria eradication (2). However, efforts to develop a successful vaccine have not yet accomplished (3). Since we need multiple vaccine candidate antigens to succeed in controlling malaria, post-genome malaria vaccine candidate discovery is necessary. One of the obstacles in this process is at the malaria protein production step and is mainly due to the lack of an efficient methodology to prepare quality proteins. *P. falciparum* genes have a very high A/T content (average 76% per coding

Y. Endo et al. (eds.), *Cell-Free Protein Production: Methods and Protocols*, Methods in Molecular Biology, vol. 607
DOI 10.1007/978-1-60327-331-2_8, © Humana Press, a part of Springer Science+Business Media, LLC 2010